# Determination of effective recombination probability: detailed aspects of a macroscopic methodology

P. Rini*and G. Degrez†
*von Karman Institute for Fluid Dynamics, 1640, Rhode-St.-Genèse, Belgium*
*Université Libre de Bruxelles, 1050 Bruxelles, Belgium*

## 1 Introduction

The purpose of the present Lecture Series is to provide an up-to-date review of the experimental techniques, the theoretical models, as well as the numerical simulation strategies involved in the treatment of the chemical character of high temperatures gases. To this end, aspects of both materials and high temperatures uid sciences are discussed together, with the aim of enhancing the improvements in the understanding of the processes of heat release on solid surfaces close to reactive gases taking place in re-usable hypersonic ight vehicles, ballistic missiles, and rockets exhaust nozzles. In addition, further details are given concerning the modeling and the experimental investigation of gas-surface interactions. This latter aspect is strongly related to the diffusive component of the heat ux experienced by a vehicle entering the atmosphere. In particular, the way in which the Thermal Protection Material (TPM) in uences the gas particle recombination on its surface has a tremendous effect on the wall heat ux. As will be shown later on, the heat ux measured in the stagnation point of a probe held in a plasma wind tunnel can simply double when materials enhancing complete recombination are used instead of inert material. Therefore, the role played by the modelling of gas/surface interactions is of fundamental importance in the understanding of heat-transfer and as a consequence in the design of Thermal Protection Systems (TPS).

When analyzing the interaction between a gas and a non ablating surface, at least two approaches can be put in evidence. A microscopic and a macroscopic approach.

Recent years have seen a very important progress in the microscopic theoretical treatment of surfaces and processes on surfaces described by the so called theoretical surface science [31]. The aim of theoretical surface science is to contribute signi cantly to the fundamental understanding of the underlying principles governing the geometric and electronic structure of surfaces, together with the processes taking place on these surfaces such as growth of surface layers, gas-surface scattering, friction or reaction at surfaces [30]. In the framework of atmospheric (re)entry, theoretical surface science could provide a very attractive tool for the improvement of the current techniques used to estimate the catalytic activity of thermal protection materials. Some research is ongoing in this direction and published data are already available providing values of recombination probabilities of oxygen on Silica based materials computed using Molecular Dynamics techniques [54]. The main advantage of this microscopic approach is that a variety of surface properties can be described from rst principles, i.e. without invoking any empirical parameters. On the other hand, this approach, based on expensive computations, has not yet been used to investigate complicated o w conditions like those typical of high enthalpy facilities. It will certainly be worth to investigate this possibility in the future.

In the eld of TPS design, a macroscopic approach is more widespread, which is closely coupled with the use and the simulation of high enthalpy plasma o ws produced in suitable facilities. In this manuscript, our attention is focused on this second way of analyzing gas-surface interactions. In particular, the methodology

*e-mail : rini@vki.ac.be
†e-mail : gdegrez@ulb.ac.be

Rini, P.; Degrez, G. (2007) Determination of Effective Recombination Probability: Detailed Aspects of a Macroscopic Methodology. In *Experiment, Modeling and Simulation of Gas-Surface Interactions for Reactive Flows in Hypersonic Flights* (pp. 15-1 – 15-46). Educational Notes RTO-EN-AVT-142, Paper 15. Neuilly-sur-Seine, France: RTO. Available from: http://www.rto.nato.int/abstracts.asp.

developed at the Institute for Problems in Mechanics (IPM) has been selected as a suitable instrument for the determination of the catalytic activity of TPM.

## 1.1 IPM Methodology to determine TPS materials catalytic activity

Within the framework of the IPM methodology, the determination of TPS materials catalytic properties rely on experimental testing on TPS materials samples in high enthalpy facilities producing o w conditions close to ight conditions. Inductively Coupled Plasma (ICP) wind tunnels are particularly suited for this purpose because they produce plasma jets of very high chemical purity, contrary to arc heated wind tunnels in which the o w is polluted by metallic impurities originating from electrode erosion, which can contaminate the TPS material sample. This was the motivation for the construction of two ICP facilities at VKI : a large scale ICP facility (Plasmatron) [6] and a small scale facility (Minitorch) [13].
Kolesnikov et al. [39, 34] proposed a methodology to estimate TPS materials catalytic activity. This methodology requires heat transfer and pitot pressure measurements on one hand, and numerical simulation of the o w in the testing facility and along the stagnation line in front of the heat transfer probe on the other hand. In the following, we present the main aspects of this methodology from the analysis of which the main motivations of this contribution were inspired.
The IPM methodology relies on a combination of heat transfer and pitot pressure measurements in a subsonic plasma jet produced in an ICP facility and numerical simulations of the o w. In this sense it represents a hybrid methodology which indeed builds on both experiments [15, 27, 40, 12, 2] and numerical simulation of high enthalpy o ws [75, 43]. Actually, the o w conditions in the ICP facility are related to ight conditions using the Local Heat Transfer Simulation (LHTS) concept [35, 3] so that the measured heat ux es are equivalent to the actual stagnation point heat ux es of a certain space vehicle at a point (altitude/velocity) of its (re)entry trajectory. A detailed description of the IPM methodology is presented in Ref. [16] and hereafter we present only its main characteristics.
This methodology, which is schematically represented in Fig. 1, is composed of the following essential building blocks:

1. An LTE with constant elemental fraction viscous o w simulation of the o w in the ICP facility heating chamber and in the downstream subsonic plasma jet. The purpose of this LTE viscous o w computation is to compute the values of the non-dimensional parameters ($\Pi_i$) which characterize the o w near the stagnation point of the heat ux probe in the plasma jet.

2. Experimental measurements of the stagnation point wall heat ux ($q_w$) and of the pitot pressure ($p$) on a cold wall ($T_w \sim 300$K) reference heat ux probe assumed to be fully catalytic[1].

3. Reconstruction of the plasma jet enthalpy and velocity gradient at the edge of the stagnation line using the measured stagnation point heat ux and pitot pressure.

4. Calculation of heat ux abacus (optional). Once the stagnation line edge conditions have been determined, the stagnation line solver can be run for various wall catalytic activity/temperature combinations to produce a heat ux abacus (set of $q_w$, $T_w$ curves at constant catalytic activity $\gamma_w$).

[1] For air o ws the material used is copper while for $CO_2$ mixtures we use Silver.

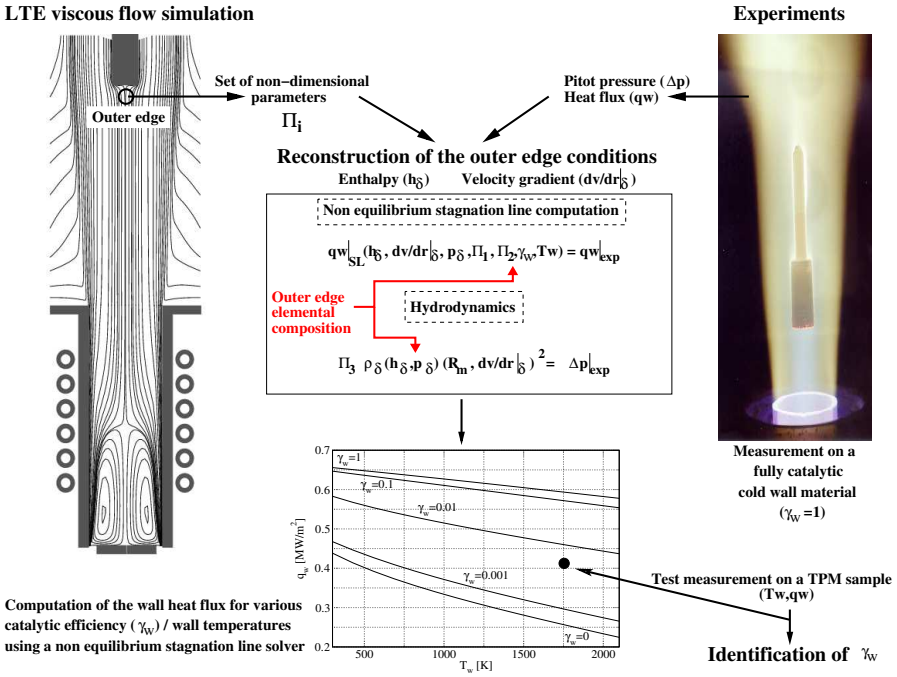


Figure 1: Schematic representation of the IPM methodology for the determination of the catalytic activity of TPS materials

5. Experimental measurement of the stagnation point heat ux to a TPS material sample and of its temperature, and determination of the material catalytic activity[2].

The previous list shows clearly the highly hybrid character of the methodology. A particular attention should be devoted to the third step, usually referred as the *rebuilding* of the outer edge conditions. The logic on which this process is based follows from the investigation of the parameters from which the stagnation point heat ux depends. Such investigation reveals that these parameters are as follows :

- the thermochemical state of the stagnation line outer edge. In the original version of the methodology the outer edge is supposed to be under thermochemical equilibrium conditions de ned by $p_\delta$, $h_\delta$, and the elemental fraction corresponding to the ICP torch inlet.
- The radial velocity gradient $[(\partial v/\partial r)_\delta]$ at the stagnation line outer edge.
- The stagnation line nite thickness ($\delta$) and the product of the normal (i.e. axial) velocity by the normal derivative of the radial velocity gradient at the stagnation line edge $[u_\delta \partial/\partial x(\partial v/\partial r)_\delta]$.
- The wall temperature ($T_w$) and the catalytic activity of the sample surface with respect to each of the $k^{th}$ possible recombination processes ($\gamma_w^k$). One of the major assumption of the original version of the

[2]This can be done graphically using the heat ux abacus by identifying the $\gamma_w$ contour on which the data point ($q_w$, $T_w$) lies, or alternatively numerically.

methodology consists in assuming all these recombination probabilities to be equal to the same effective probability $\gamma_w$.

Among these parameters, only two are unknown : the outer edge enthalpy ($h_\delta$) and the radial velocity gradient [$(\partial v/\partial r)_\delta$]. Indeed, the stagnation pressure ($p_\delta$) and the wall temperature ($T_w$) are known experimentally, the recombination probability ($\gamma_w^k = \gamma_w \; \forall k$) is equal to one according to the assumption of a fully catalytic heat ux probe. In addition, the stagnation line thickness ($\delta$) and $u_\delta \partial/\partial x(\partial v/\partial r)_\delta$ are related to the radial velocity gradient itself and to the probe radius $R_m$ through the non-dimensional hydrodynamic parameters obtained from the simulation of the plasma o wing in the ICP facility performed assuming thermochemical equilibrium conditions with constant elemental fraction to be established both in the torch and in the test chamber. The rst two non dimensional parameters[3] read as follows :

$$\Pi_1 = \frac{\delta}{R_m} \qquad \Pi_2 = u_\delta \frac{\partial}{\partial x}\left(\frac{\partial v}{\partial r}\right)_\delta \Big/ \left(\frac{\partial v}{\partial r}\right)^2, \tag{1}$$

so that the stagnation point heat ux can be determined from the solution of the stagnation line problem (SL) which implicitly reads

$$q_w(\underbrace{h_\delta, \left(\frac{\partial v}{\partial r}\right)_\delta}_{\text{unknown}}, p_\delta, \Pi_1, \Pi_2, \gamma_w, T_w). \tag{2}$$

The additional equation needed to retrieve the two unknowns ($h_\delta$, $(\partial v/\partial r)_\delta$) is given from the knowledge of the measured pitot pressure. This measurement is related to $\rho_\delta$ and $(\partial v/\partial r)_\delta$ through a third non-dimensional hydrodynamic parameter obtained from the LTE viscous o w simulation carried out assuming constant elemental fraction, i. e.

$$\Pi_3 = \frac{\Delta p}{\rho_\delta(h_\delta, p_\delta)[R_m(\partial v/\partial r)_\delta^2]}. \tag{3}$$

The two unknown o w quantities are then determined by solving the system (2)-(3) by some suitable iterative scheme, relying on the fact the functional form (2) is provided implicitly by running a non-equilibrium stagnation line solver[4].

In this paper we wish to investigate and solve some of the issues previously described by merging and exploring some of the ideas scattered in the literature, and at the same time present and recommend new concepts. The outcome of this process consists in the proposition of a modi cation to the IPM methodology for the determination of the catalytic properties of TPS materials, based on the investigation of its main weak points. The determination of these weak points follows directly from the description presented in the previous section. Indeed, we notice that several conditions must be satis ed in order for the methodology to be successful :

[3]For the computation of the non-dimensional parameters it is necessary to de ne the location of the stagnation line outer edge. This position is selected to be coincident with the in ection point of the axial velocity pro le along the stagnation line obtained from the inductively coupled plasma o w simulation. Further details about the theoretical background on which this choice is based are given in Ref. [37], while the low sensitivity of the $\Pi_i$ to the choice of $\delta$ has been veri ed in Ref. [71]

[4]A slightly different approach, involving an additional dependent non-dimensional parameter, is proposed in the original version of the IPM methodology [16] and implemented in the VKI-Rebuilding code [28].

- the plasma flow in the ICP facility should be under thermochemical equilibrium and elemental diffusion should not affect the flow solution.
- The stagnation line flow should be under chemical non equilibrium to make the wall heat flux sensitive to variations in the surface catalytic activity.
- The recombination probability of all heterogeneous recombination processes should be the same.

The investigation of the validity of some of the assumptions/conditions previously listed represented the main *motivation* and *objective* of the present study and lead us to the following main contributions of our work.

- In the past, not sufficient credit has been given to the phenomenon of elemental diffusion within the atmospheric (re)entry related literature. Indeed, in a wide variety of applications, this phenomenon has been neglected. In particular, this is the case in the IPM methodology. The investigation of this aspect of high temperature flow modeling leads us to the derivation of an explicitly closed form of the governing equations of mixtures of reacting gases under LTE presented in Sec. 2. This was possible reducing the equations of chemically reacting flows to an elegant system consisting of the conventional Navier-Stokes equations (mass, momentum, energy) complemented by an advection-diffusion equation for the mass fraction of each chemical element in the mixture. The obtained formalism is in closed form in the sense that diffusive fluxes are directly expressed in terms of gradients of the solution unknowns, unlike other formulations in which these fluxes are obtained in an implicit manner, by solving the full system of Stefan-Maxwell equations. The main contribution of this formalism consists in the introduction of several new LTE transport coefficients.
- In Sec. 3 we present an application of the derived theory to the description of $CO_2/N_2$ LTE mixtures flowing along a stagnation line. This leads to the original computation of multicomponent elemental diffusion coefficients for mixtures containing more than two elements.
- In Sec. 4 we investigate the effects of elemental diffusion on the behavior of air and $CO_2$ plasmas flowing within the VKI-Plasmatron in a certain range of operating conditions. In addition we provide a characterization of hot air jet flowing into the test chamber of the VKI-Plasmatron facility. This study suggest a modification of the original version of the IPM methodology based on the observation that, for sufficiently high operating pressures, chemical equilibrium conditions with variable elemental fraction are established within the torch and the test chamber. As a consequence, the stagnation line outer edge elemental fractions should be added to the set of non-dimensional parameters ($\Pi_i$) needed in the rebuilding process.
- In Sec. 5 an alternative model for the phenomenological description of gas-surface interactions is presented and tested in the framework of TPM catalycity determination for Mars entry applications.

# 2 Theory of LTE viscous flows with variable elemental fractions

The physics of collision-dominated chemically reacting flows is described by an extended Navier-Stokes system, consisting of the following equations [67]: global continuity; momentum and total energy; a separate continuity equation for each species, including finite-rate chemistry; if thermal non equilibrium occurs, an energy equation for each additional mode of freedom (vibrational, rotational and electronic energies).
This formalism has several drawbacks. Firstly, the equations are costly to implement and solve numerically. Secondly, many physical parameters essential for the modeling of chemistry and energy relaxation processes are usually missing. Thirdly, even when a numerical solution is obtained, it is by no means obvious to interpret the vast amount of information obtained (e.g. concentration fields of a large number of chemical species). For these reasons, when chemistry and energy exchanges are fast, it is usually preferable to solve the more elegant and less uncertain Local Thermodynamic Equilibrium (LTE) form of the aforementioned set of equations.
A major breakthrough in the field of LTE flow modeling was made by Butler and Brokaw [9, 7], who showed that, assuming vanishing diffusive fluxes of chemical elements, the diffusive transport of species reaction enthalpies in the energy equation could be incorporated in a straightforward manner by introducing a coefficient of 'thermal reactive conductivity' $\lambda_R$:

$$\sum_{s=1}^{N_{sp}} \mathbf{W}_s h_s = -\lambda_R \nabla T. \tag{4}$$

One often makes use of this result to reduce the full set of non equilibrium equations to a system formally equivalent to the 'conventional' Navier-Stokes equations (continuity, momentum and energy), complemented by a modified equation of state $\rho(p,T)$ computed from statistical mechanics assuming a fixed elemental composition in the flow. For instance, Vasil'evskii et al. [77] successfully used this classical LTE formalism to simulate high-pressure air inductively coupled plasma flows, imposing a 21/79 volumetric ratio of oxygen and nitrogen elements throughout the flow field. While appealing because of its simplicity, it is important to understand that this approach is approximate at best, since in general the elemental composition varies significantly in chemically reacting flows. Over the past four decades, several LTE formulations accounting for (de)mixing effects have been proposed in several contributions [48, 23, 24, 25, 26, 55, 70, 32, 22, 72, 73, 78, 68, 41, 45, 46, 48, 47, 18, 74, 59, 58, 64], a description of which is proposed in Ref. [57]. In the remaining part of the section we will firstly present a preliminary analysis of the influence of elemental demixing on the behavior of a mixture of reacting gases by computing the composition for a fixed pressure and several elemental compositions, in the range of temperatures [300 K,15000 K] typical of applications to TPS testing. Secondly we will recall the theory of LTE viscous flows with variable elemental fractions for neutral mixtures derived in Ref. [62], referring the extension to mixtures of ionized species to Ref. [57]. Although we will focus on the particular case of air and carbon dioxide mixtures, well-suited for Earth and Mars entry applications, we wish to point out that the presented LTE formulation is applicable to any chemically reacting flow near LTE and in particular the hydrocarbon-air mixtures used for combustion.

## 2.1 Influence of elemental fractions on thermochemical equilibrium composition

It is well known that the composition of a mixture of reacting gases under thermochemical equilibrium can be expressed as a function of pressure, temperature, and of the elemental fractions of the elements shared among

the mixture species [79, 1]. The contents of this section deal mainly with the issue of elemental fraction variations in reacting flows under LTE. To attract the readers's interest, we present a preliminary analysis of the influence of elemental fraction variations on the mixture composition for both air and carbon dioxide mixtures. As a result we show that a 10% variation of oxygen elemental fraction can induce a 50% difference in the species concentration for $CO_2$ mixtures.

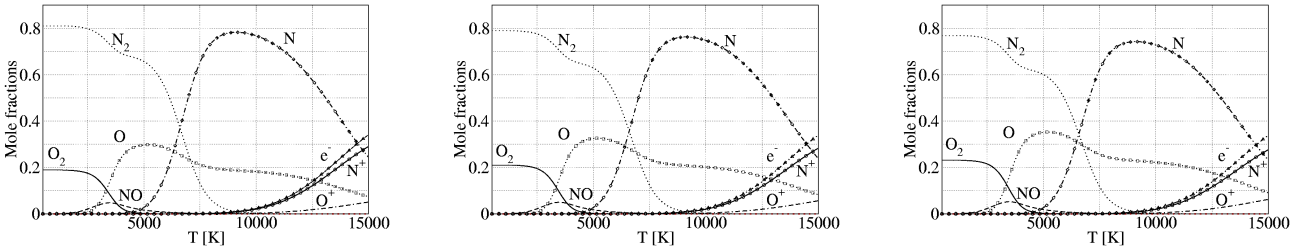


(a) **Mole fractions ($X^0$ = 0.189, $X^N$ = 0.811).** (b) **Mole fractions ($X^O$ = 0.21, $X^N$ = 0.79).** (c) **Mole fractions ($X^O$ = 0.231, $X^N$ = 0.769).**

(d) **Mole fractions ($X^O = \frac{18}{30}$, $X^C = \frac{12}{30}$).** (e) **Mole fractions ($X^O = \frac{2}{3}$, $X^C = \frac{1}{3}$).** (f) **Mole fractions ($X^O = \frac{22}{30}$, $X^C = \frac{8}{30}$).**

Figure 2: Influence of elemental fractions on thermochemical equilibrium composition for air and carbon dioxide mixtures. (p=1 atm)

Consider an air mixture composed by the following 11 species : $N_2, O_2$, NO, N, O, $N_2^+$, $O_2^+$, $NO^+$, $N^+, O^+, e^-$. Let us define a reference mixture characterized by elemental fractions $X^O = 0.21$, $X^N = 0.79$, and two additional mixtures obtained by perturbing the oxygen fraction by an amount of ±10%, i.e. $X^O = 0.231$, $X^N = 0.769$ and $X^O = 0.189$, $X^N = 0.811$. In Figs. 2(a), 2(b), and 2(c) the composition of these mixtures is shown as a function of temperature for a fixed pressure equal to 1 atm, assuming thermochemical equilibrium conditions. From these figures appear that the species mole fraction is little affected by the elemental fraction, whose influence is basically limited to a scaling of the various species according to the elemental fraction. The reason is because in the air mixture, there are only 2 species including both N and O atoms, i.e. NO and $NO^+$, and in addition their concentration always remains small.

For carbon dioxide mixtures, the sensitivity of the chemical composition to elemental fraction variations is much higher than for air. Indeed, if one considers an 8 species mixture [59] in chemical equilibrium composed by $CO_2$, $O_2$, CO, C, O, $C^+$, $O^+$, and $e^-$, and computes the chemical composition as a function of temperature for a fixed pressure, very different results are obtained depending on the elemental fraction used. Consider a reference mixture characterized by elemental fractions $X^O = \frac{2}{3}$ and $X^C = \frac{1}{3}$. Perturbing by ±10% the oxygen fraction, two new mixtures are defined: $X^O = \frac{22}{30}$, $X^C = \frac{8}{30}$ and $X^O = \frac{18}{30}$, $X^C = \frac{12}{30}$. The mole fraction evolution as a function of temperature, for a pressure of 1 atm, for these three cases is shown in Figs. 2(d), 2(e), and 2(f). A

very strong in uence of the elemental fraction on the chemical composition is clearly visible. Moreover, from the analysis of the previous results, it follows that, in the case of $CO_2$ mixtures, the sensitivity to elemental fraction variation is much higher than in the case of air.
This will result in an important in uence of elemental demixing on heat ux in thermochemical equilibrium $CO_2$ mixtures, as will be shown by the results to be presented later on.

## 2.2 Mixtures of neutral species

### 2.2.1 Species ordering and nomenclature

We represent mixtures of perfect gases by means of a nite set of $N_{sp}$ species $\tilde{\mathcal{S}}$, amongst which we furthermore distinguish between $N_c$ 'independent species' $\tilde{\mathcal{E}}$ consisting of pure elements (as such as in their stable form) and $N_r$ 'combined species' $\tilde{\mathcal{R}}$, for instance:

**5-species air** $\tilde{\mathcal{E}} = \{O, N\}$, $\tilde{\mathcal{R}} = \{O_2, N_2, NO\}$, and $\tilde{\mathcal{S}} = \tilde{\mathcal{R}} \cup \tilde{\mathcal{E}}$,

valid for LTE mixtures at pressures above 0.01atm and for temperatures between 300 and 8000 K. We accordingly de ne the three sets of indexes $\mathcal{R} = \{1, \ldots, N_r\}$, $\mathcal{E} = \{N_r + 1, \ldots, N_{sp}\}$, and $\mathcal{S} = \mathcal{R} \cup \mathcal{E}$. We characterize the chemical composition of the mixture in terms of mole fractions $x_s = n_s/n$, where $n_s$ and $n$ stand for the molar densities of individual species and of the entire mixture. Alternatively, we can also characterize the mixture composition by means of the mass fraction $y_s = \rho_s/\rho$, where $\rho_s$ and $\rho$ stand for the mass densities of the individual species, respectively the full mixture.
We will indicate the number of atoms of element $e$ contained in a species $s$ by $\phi_s^e$, for instance, for NO, $\phi_3^5 = 1$ while for $O_2$ $\phi_1^4 = 2$. This enables us to de ne the mole fractions $X^e$ and mass fractions $Y^e$ of elements in the mixture as follows:

$$X^e = \frac{\sum\limits_{s\in\mathcal{S}} \phi_s^e x_s}{\sum\limits_{e\in\mathcal{E}} \sum\limits_{s\in\mathcal{S}} \phi_s^e x_s}; \qquad Y^e = \sum_{s\in\mathcal{S}} \phi_s^e y_s \frac{M_e}{M_s}, \tag{5}$$

where $M_s$ is the molar mass of species $s$, related to the mixture molar mass $M = \sum_{s\in\mathcal{S}} x_s M_s$. We introduce the diffusion velocity $\mathbf{V}_s$ with respect to the mass-averaged velocity of the mixture $\mathbf{u}$. The molar and mass ux es of species $s$ are then given by respectively $\mathbf{W}_s = n_s\mathbf{V}_s$ and $\mathbf{J}_s = M_s n_s \mathbf{V}_s$.The mole and mass ux es of element $e$ are then given by

$$\mathbf{N}_e = \sum_{s\in\mathcal{S}} \phi_s^e \mathbf{W}_s; \qquad \mathcal{J}_e = M_e \mathbf{N}_e \qquad (e \in \mathcal{E}). \tag{6}$$

We use bold type fonts to indicate vectors in the physical space. With 'bar notation', we refer to arrays containing species, elemental or reactive properties, with respective lengths of $N_{sp}$, $N_c$ and $N_r$.

### 2.2.2 Computation of composition under LTE

**Species continuity equations**

We consider the commonly encountered flow regime in which chemical reactions are relatively rare w.r.t. elastic collisions, such that they do not play an important role in the thermalization of species in the flow (unlike the 'kinetic chemical equilibrium regime' considered in the first part of Ref. [18], for which chemical reactions and elastic collisions are treated on the same level). The concentration of each species may then be determined from a respective species continuity equation [67]:

$$\partial_t(\rho y_s) + \nabla\cdot(\rho y_s \mathbf{u}) + \nabla\cdot(M_s \mathbf{W}_s) = \omega_s \tag{7}$$

where $\mathbf{u}$ stands for the mass-averaged velocity of the mixture and $\omega_s$ is the mass production/destruction term [79] of species $s$ due to chemical reactions. The number fluxes of species respect the mass conservation constraint

$$\sum_{s\in\mathcal{S}} M_s \mathbf{W}_s = 0 \tag{8}$$

and obey the Stefan-Maxwell equations [22, 32]

$$\frac{M}{\rho}\sum_{k\in\mathcal{S}} \frac{x_s\mathbf{W}_k - x_k\mathbf{W}_s}{\mathcal{D}_{sk} f_{sk}(L)} = \nabla x_s \tag{9}$$

for $s \in \mathcal{S}$. To keep the analysis as simple as possible, we have neglected effects of pressure and thermal diffusion; note however that these could be included without any particular problem as shown in Ref. [57].

**Elemental continuity equations for neutral mixtures**

As pointed out by Murphy, we need to solve additional element advection-diffusion equations to determine the elemental composition of the mixture [46, 58]. The solution of these equations will then be used, together with two independent thermodynamics variables, temperature and pressure for example, to compute the mixture composition as the solution of a non-linear system [79]. To obtain these equations, we multiply Eqs. (7) by $\phi_s^e M_e/M_s$ and sum over all species. Since no elements are created in the considered chemical reactions, the mass fraction of any element $e$ obeys the following equation:

$$\partial_t(\rho Y^e) + \nabla\cdot(\rho \mathbf{u} Y^e) + \nabla\cdot\mathcal{J}_e = 0 \qquad (e \in \mathcal{E}). \tag{10}$$

In Ref. [62] we have shown that under LTE conditions, the mass diffusion flux of elements $\mathcal{J}_e$ can be expressed in terms of gradients of elemental mass fractions and temperature. For simplicity, we consider flows at constant pressure, consistent with the neglect of pressure diffusion in Eqs. (9). Once again, we remark that this does not imply any fundamental limitation and pressure diffusion could be included easily if needed (see Ref. [57]). Following the approach proposed in Ref. [62], the elemental diffusive fluxes are expressed introducing the

elemental multicomponent diffusion coefficients $D_{ef}$ and thermal demixing coefficients $D_e^T$. This lead to the following expression for the elemental diffusive ux es :

$$\mathcal{J}_e = -\sum_{f\in\mathcal{E}} \rho D_{ef} \nabla Y^f - \rho D_e^T \nabla T. \tag{11}$$

The second term in the right hand side of the above result will in general generate nonzero elemental diffusion ux es even when the initial elemental composition is uniform.

### 2.2.3 Diffusive transport of enthalpy

In reacting o ws, the diffusion of species affects the mixture energy balance through the heat ux term:

$$\mathbf{q}_d = \sum_{s\in\mathcal{S}} \mathbf{W}_s h_s. \tag{12}$$

In a general non equilibrium case, to compute $\mathbf{q}_d$, one should determine all the $\mathbf{W}_s$ as a solution of Eq. (9) and then compute the above linear combination, as done in the methodology of Refs. [70],[18] and [58]. On the other hand, under thermochemical equilibrium, Eq. (12) can be cast under a particular form which avoids the computation of the $\mathbf{W}_s$. A rst step in this direction was made by Butler and Brokaw [9], who showed that, under the assumption of vanishing elemental ux es, the diffusive heat ux takes the form of Eq. (4). In this section, we extend the work of Butler and Brokaw to the more general case when elemental ux es are nonzero. As shown in Ref. [62], for a mixture of reacting gases under thermochemical equilibrium, at constant pressure, the diffusive heat ux is proportional to both temperature and elemental concentration gradients, and can be expressed as:

$$\sum_{s\in\mathcal{S}} \mathbf{W}_s h_s = -(\lambda_R + \lambda_D)\nabla T - \sum_{e\in\mathcal{E}} \lambda_{EL}^e \nabla Y^e. \tag{13}$$

From Eq. (13), we see that in an LTE o w, the diffusive heat ux vector consists of three different parts:

(1) the ‘thermal reactive conductivity’ coefficient $\lambda_R$ is identical to the well-known results by Butler and Brokaw [9, 7] and takes into account diffusive transfer of species enthalpies in the absence of elemental diffusion.

(2) The ‘thermal demixing conductivity’ coefficient $\lambda_D$ corrects for the additional diffusive heat transfer that occurs due to nonzero elemental diffusive ux es when elemental mass fraction gradients are zero.

(3) Finally, the ‘elemental heat transfer coefficients’ $\lambda_{EL}^e$, take into account heat transfer due to elemental demixing driven by gradients in elemental composition.

In the next section we will present an application of this formulation to investigate diffusion phenomena along the stagnation line present in front of a probe placed in the test chamber of an inductively coupled plasma facility.

# 3 Diffusion phenomena in reacting mixtures : applications to stagnation line flows

This section is inspired by the research presented in Ref. [63], where the authors present a detailed analysis of diffusion phenomena in flows of reacting mixtures along a stagnation line present in front of a probe placed in the test chamber of an inductively coupled plasma facility. In the following we limit our description to the presentation of the results of the solution of the stagnation line differential problem and we refer the interested reader to our previous publications [59, 58, 57] for a detailed presentation of the stagnation line equations. In these references we also discuss the models used for the computation of the transport and thermodynamics properties of reacting mixtures such as those used to obtain the following results.
The following mixture has been selected as representative for Mars entry :

**Mars-8 species :** $\mathcal{E} = \{C, N, O\}, \mathcal{R} = \{CO_2, CO, O_2, N_2, NO\}$.

The computations carried out using the Mars-8 mixture represent a direct application of the theory presented in Sec. 2. This represents the first attempt to simulate mixtures of hetero-nuclear molecules with more than two elements using the closed form of the equations derived in Ref. [62]. The use of the theory presented in Sec. 2, will moreover allow to show the improvements brought by the theory itself in terms of physical understanding of the flow behavior. Although stagnation line flows are often under chemical non equilibrium conditions, our previous analysis [58] showed that for a $CO_2$ mixture, assuming a fully catalytic wall provides an estimation of wall heat flux close to the one obtained by assuming LTE conditions to be established along the stagnation line, provided that elemental demixing is taken into account. In addition, the elemental fraction profiles obtained under chemical non equilibrium follow closely those under chemical equilibrium. Thus we will present the solution of the LTE stagnation line problem formulated following the equations presented in Ref. [57].
To present our analysis of the stagnation line flow we will start defining the test case to be investigated and then the solution of the stagnation line flow will be presented with strong emphasis on the description of diffusion phenomena.

## 3.1 Test case definition

The flow conditions considered, characteristic of Martian entry [66], are presented in Table 1.
The presented outer edge conditions and geometrical parameters, have been determined from a detailed numerical [33] study of the flow field inside the inductively coupled plasma generator and test chamber of the VKI's plasmatron wind tunnel [5]. This allows for the computation of some non-dimensional parameters related to the stagnation line edge in terms of the boundary layer thickness, the axial velocity, and the velocity gradient and further details about their definition are available in previous publications [16].
In the following a single chemical regime is considered, corresponding to LTE with variable elemental fraction (LTE-VEF), where the flow is in thermochemical equilibrium and the composition is computed as a function of pressure, temperature, and local elemental fractions, obtained from the solution of the set of elemental continuity equations. Two formulations have been used.

Table 1: Operating Conditions.

| | |
|---|---|
| $T_w$ [K] | 300 |
| $T_\delta$ [K] | 5827 |
| $p_\delta$ [Pa] | 7000 |
| $R_m$ [mm] | 25 |
| $\delta$ [mm] | 9 |
| $v_\delta \partial/\partial y(\partial u_\delta/\partial x)/(\partial u_\delta/\partial x)^2$ [-] | 1.77 |
| $\partial u_\delta/\partial x$ [$s^{-1}$] | 913 |

**LTE-VEF (1)** we obtain the elemental concentration by solving Eqs. (10), where the element diffusive ux es are computed as a linear combination of the species ones obtained as the solution of the Stefan-Maxwell equations [Eq. (9)]. The computed species diffusive ux es are then used in the energy equation to evaluate the diffusive transport of enthalpy [58] ($\sum J_s h_s$).

**LTE-VEF (2)** we obtain the elemental concentration by solving Eqs. (10), where the thermal demixing and multicomponent diffusion coefficients are used to compute the element diffusive ux es [Eq. (11)]. Moreover, an alternative form of the energy balance, based on the use of Eq. (13) is used, introducing the correction to $\lambda_R$ as well as the elemental heat transfer coefficients.

### 3.2 Stagnation line solution

In this section we present the solution of the stagnation line equations for the conditions speci ed in Tab. 1. We start our analysis by discussing the temperature and enthalpy pro les shown in Fig. 3(a).
There we present the results obtained for the LTE-VEF regime using the two formulations LTE-VEF (1) and LTE-VEF (2) previously de ned. As observed, the results obtained with the two formulations are identical. The same match is observed for all o w variables along the stagnation line, supporting the correctness of the alternative formulation recalled in Sec. 2.
In Fig. 3(b) we present the species concentration pro les. Starting from CO, O, C, and N at the outer edge, we see how their concentration decreases providing a mixture of $CO_2$, $O_2$, $N_2$ at the wall and a small amount of NO. From the analysis of this picture, it appears that elemental demixing tends to reduce the amount of carbon and nitrogen at the wall while it enhances the oxygen concentration. This is re ected by the presence of an excess of $O_2$ in the low temperature region, which would have been zero if the wall elemental fractions had been the same as at the outer edge. This behavior is con rmed by the pro les presented in Fig. 3(c), where we plot the difference between the local elemental mass fractions and their outer edge values [$Y^e(y)$-$Y^e|_\delta$]. In addition, by looking to the element concentration pro les [Fig. 3(c)] we notice that the lack of carbon and nitrogen at the wall is compensated by a higher concentration around $y/\delta = 0.4$, while for oxygen we observe a minimum in this position and a subsequent concentration rise as the wall is approached.
Going further with the analysis of the pro les presented in Fig. 3(c), we notice that they present a non-monotone behavior and hereunder we give an alternative explanation for this observation. To discuss the elemental mass fraction behavior we focus on the elemental continuity equations [Eq. (10)]. It is clear how the knowledge of

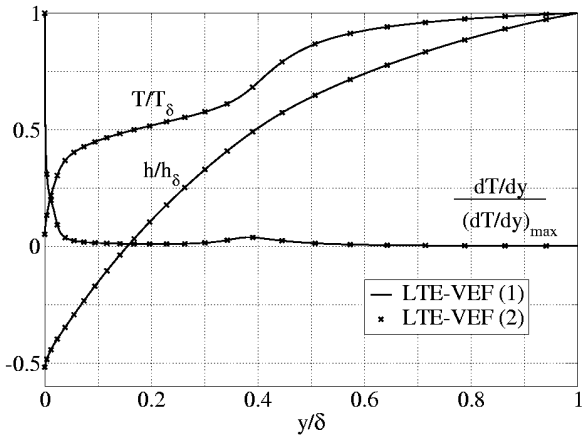


(a) **Temperature and enthalpy pro les.**

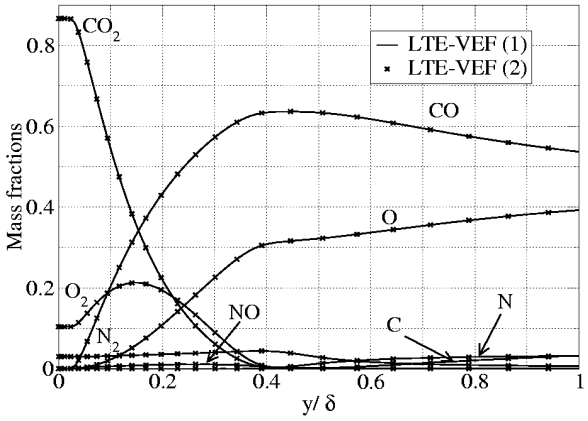


(b) **Species mass fractions.**

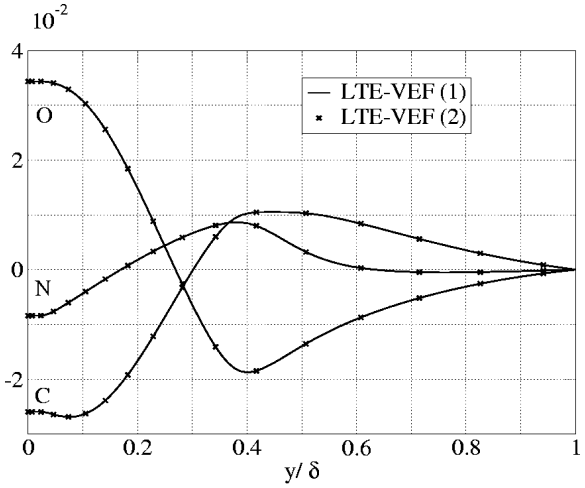


(c) **Difference between the elemental mass fractions and their outer edge values ($Y^e(y)$-$Y^e|_\delta$).**

Figure 3: Comparison of the computed results along the stagnation line obtained using the LTE-VEF (1) and the LTE-VEF (2) formulations.

$\mathcal{J}_e$ will help understanding the evolution of $Y^e$ knowing that the velocity is aligned with the stagnation line and directed towards the wall.

For this purpose we present the pro les of $\mathcal{J}_e$ in Fig. 4 for the three elements contained in the mixture. As expected [Eq. (10)] we observe a correspondence between the local extrema of $\mathcal{J}_e$ and those of $Y^e$. In addition, we notice that the diffusive ux es of elements are zero all over the rst 10% of the stagnation line and they start to grow around $y/\delta \approx 0.1$. This shows that over the rst 10% of the stagnation line, Eq. (10) simpli es to $\mathcal{J}_e = 0$, meaning that convection is by far negligible. Moving further towards the outer edge a local extremum is encountered, followed by an increase for C and N, while for oxygen a decrease of $\mathcal{J}_O$ is observed. From this we notice that in the region de ned by $y/\delta > 0.1$, the convective term will differ from zero and will counteract the derivative of the pro les presented in Fig. 4. At this point, it is important to observe that, although the pro les of Fig. 4 allow the interpretation of the elemental fraction pro les presented in Fig. 3(c), it is by no

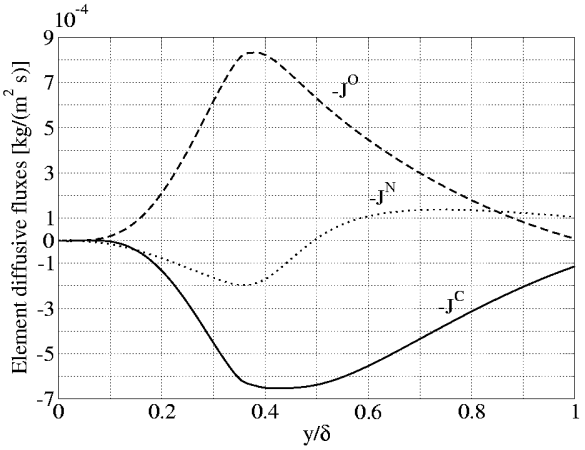


Figure 4: Elemental diffusive ux es ($-\mathcal{J}_e$).

means evident to give an explanation for the behavior of the $\mathcal{J}_e$ if they are computed as a linear combination of the solutions of Eqs. (9) as done in the formulation LTE-VEF (1) [58, 64]. Now, to improve our understanding, we use the theory introduced in Sec. 2 and applied in the LTE-VEF (2) formulation of the equations.

Indeed, to understand the behavior of the element diffusive ux es we discuss now the two components of $\mathcal{J}_e$. The rst proportional to the temperature gradient ($\rho D_e^T \nabla T$) and the second obtained as a linear combination of the element mass fractions gradients ($\rho \sum D_{eq} \nabla Y^q$). In Fig. 5(a), we present the rst part of the element diffusive ux es. From Fig. 3(a) we notice that $\partial T/\partial y > 0 \ \forall y$ and therefore the sign of $\rho D_e^T \nabla T$ will depend only on $D_e^T$, $\rho$ being obviously a positive quantity.

As shown in Ref. [62, 63] and con rmed in Fig. 5(b), the $D_e^T$ change their sign as temperature rises, for x ed pressure and elemental fractions. In the present case, the pressure is constant along the stagnation line but the elemental fraction varies. Therefore, both temperature and elemental composition will in uence the transport properties and therefore concur to the establishment of the pro les presented in Fig. 5(a).

Close to the wall, the thermal demixing coefficients are zero and do not contribute to the element diffusive ux es. As temperature rises, we observe an increase in module of all contributions until a maximum is reached. Then we notice a decrease and a subsequent change in sign typical of the thermal demixing coefficients behavior.

Indeed, from Fig. 5(b), we see how the behavior of the thermal demixing coefficients is similar to the one of the rst contribution to the element diffusive ux es.

In Fig. 5(c), we plot the second contribution to the elemental diffusive ux es. Also this contribution starts from zero at the wall and follows a non monotone behavior passing through a change in sign for O and C. The change in sign observed for the second contribution to the elemental diffusive ux es is not due to the elemental multicomponent diffusion coefficients but to the elemental mass fractions. Indeed, as shown in Ref. [63] and observed in Fig. 5(d), the multicomponent diffusion coefficients have the same sign in the temperature range of interest. This allows for the following interpretation of diffusion phenomena along the stagnation line. Since temperature decreases from the outer edge towards the wall, the temperature gradient is always positive along the stagnation line. In sufficiently low temperature regions, where chemical reactions do not occur, the thermal demixing coefficients are zero and do not induce demixing. As a consequence, since elemental multicomponent diffusion coefficients are not zero at low temperatures, the elemental composition stays constant ensuring mass

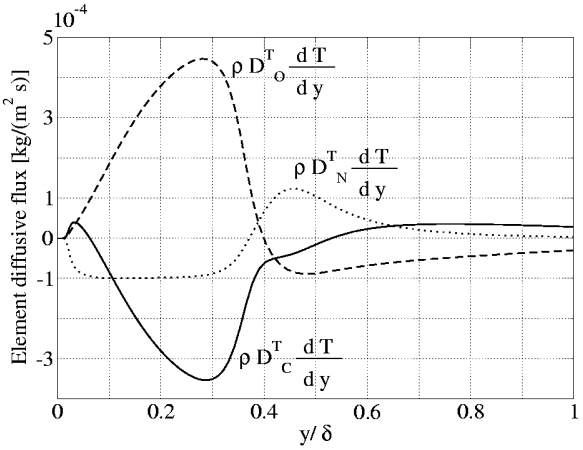


(a) **First contribution to the element diffusive uxes ($\rho D_e^T \nabla T$).**

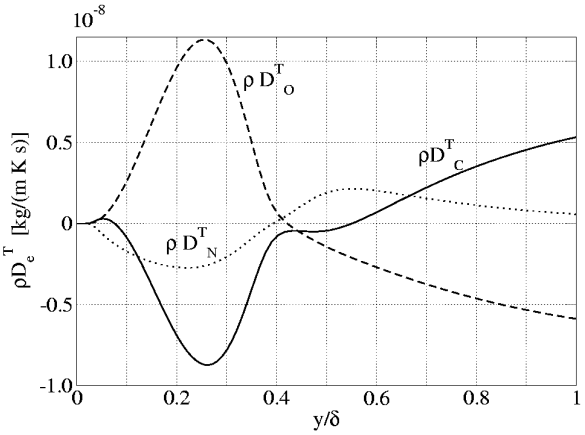


(b) **Thermal demixing diffusion coefficients.**

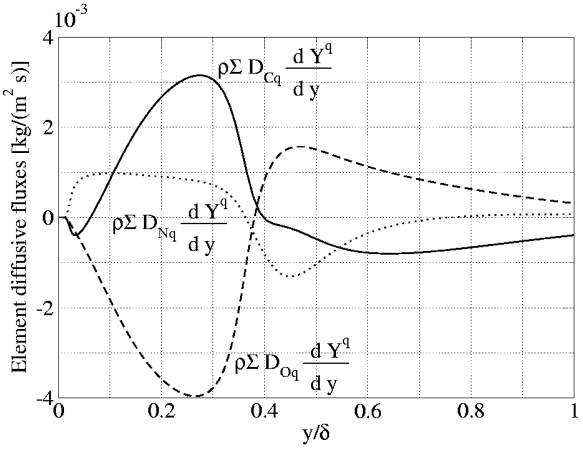


(c) **Second contribution to the element diffusive uxes ($\rho \sum D_{eq} \nabla Y^q$).**

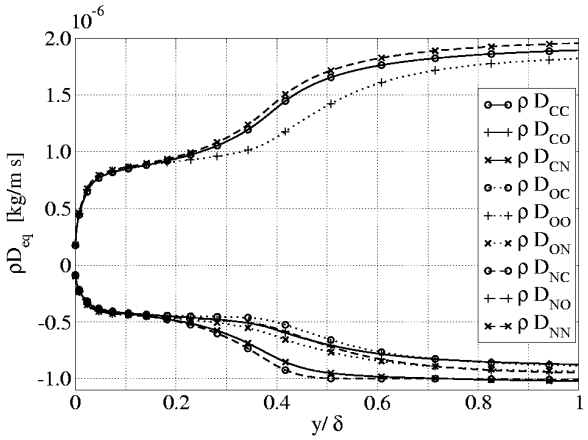


(d) **Multicomponent elemental diffusion coefficients.**

Figure 5: Elemental diffusive ux components, elemental multicomponent and thermal diffusion coefficients.

conservation ($\mathcal{J}_e|_w = 0$). As we move away from the wall ($y < 0.05$), the thermal demixing coefficients causes a non zero contribution to the elemental diffusion ux which tends to decrease oxygen concentration ($D_O^T > 0$), increase nitrogen concentration ($D_N^T < 0$), and slightly decrease but then increase again carbon concentration ($D_C^T > 0$ and $D_C^T < 0$). As soon as variations in elemental composition are induced ($\nabla Y^e \neq 0$), a counteracting contribution to the element diffusive ux es appear which tends to smooth out elemental concentration pro les until the outer edge is reached. In the central part of the stagnation line, the two contributions to element ux es interact until the point in which the thermal demixing coefficients change sign. There, to counteract this demixing term, the sign of element concentration gradients needs to change since the multicomponent diffusion coefficients have a constant sign [Fig. 5(d)]. The counteracting character of the term $\sum \rho D_{eq} \nabla Y^q$ with respect to $\rho D_e^T \nabla T$ justify its label of 'mixing term' and the comparison of Figs. 5(a) and 5(c) clearly shows this behavior. The mathematical origin of this diffusive character of the mixing term has to be searched in the non negativity of the matrix containing the elemental multicomponent diffusion coefficients. To prove the latter property of the

matrix $D_{eq}$ we computed its eigenvalues along the stagnation line. Since this matrix is singular [$\sum_{q\in\mathcal{E}} D_{eq} = 0$], one eigenvalue is $k_1 = 0$ and the remaining two $(k_2, k_3)$ have been found to be positive and monotonically increasing as a function of $y$ [63]. This result shows the non negative character of the matrix $D_{eq}$.
As a summary, we wish to point out that, from the knowledge of the set of transport properties including both elemental thermal demixing and multicomponent diffusion coefficients, we can justify the evolution of the diffusive ux es and therefore understand the shape of the elemental fractions pro les one can observe in the solution of the stagnation line problem.

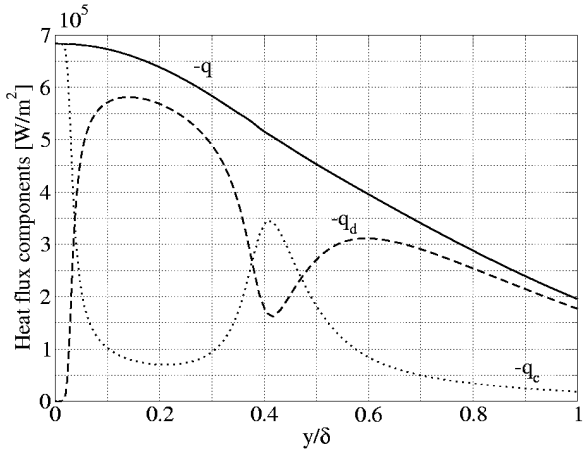


Figure 6: Heat ux components.

We now move to the analysis of the heat and mass transfer along the stagnation line by means of conduction and diffusion. As shown in Sec. 2, under the assumption of local thermodynamic equilibrium, the diffusive transport of enthalpy can be split into two parts related to $\nabla T$ and $\nabla Y^q$ respectively. As a consequence, as shown in Eq. (2), the computation of the heat ux involves the determination of two terms one proportional to the temperature gradient $[-(\lambda + \lambda_R + \lambda_D)\nabla T]$ and the other proportional to the linear combination of element concentration gradients $[-\sum \lambda^q_{EL} \nabla Y^q]$. Moreover, the heat ux in a mixture of reacting gases is composed of a conductive part ($\mathbf{q}_c = -\lambda \nabla T$), to which the diffusive transport of enthalpy needs to be added ($\mathbf{q}_d = \sum h_s \mathbf{J}_s$). To investigate the heat ux along the stagnation line and highlight the relative importance of the various contributions we start presenting the evolution of $\mathbf{q}$, $\mathbf{q}_c$, and $\mathbf{q}_d$ along the stagnation line in Fig. 6. There we observe that the total heat ux presents an increasing monotone behavior starting from the outer edge until the wall, acting to balance the convection of enthalpy. At the same time we notice that this smooth evolution appears to be the result of a quite complex shape of the two contributions $\mathbf{q}_c$ and $\mathbf{q}_d$ presented in the same gure. This highly non-linear behavior of the two heat ux components is the result of the evolution of six transport coefficients $(\lambda, \lambda_R, \lambda_D, \lambda^q_{EL})$ and four gradients $(\nabla T, \nabla Y^q)$. To provide an exhaustive description of the heat ux along the stagnation line, we start investigating the behavior of the three thermal $(\lambda)$, thermal reactive $(\lambda_R)$ and demixing $(\lambda_D)$ conductivities shown in Fig. 7(a).
As expected, we notice $\lambda_R$ to be the major contribution to the rst part of the heat ux followed by $\lambda$. We also notice that $\lambda_D$ has a non-monotone behavior including changes in sign, highlighting the fact that demixing tends to increase or decrease heat ux depending on the local temperature and elemental fractions as already observed in Ref. [64]. Moreover, in terms of heat ux intensity, we notice that around $y/\delta = 0.3$, $\lambda_D \approx \lambda$ showing how, neglecting $\lambda_D$ with respect to $\lambda$ could lead to important errors. The knowledge of the evolution of the transport

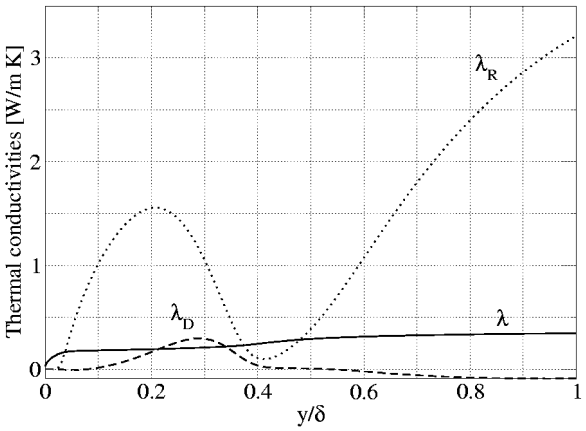


(a) **Thermal, reactive, and demixing conductivities along the stagnation line.**

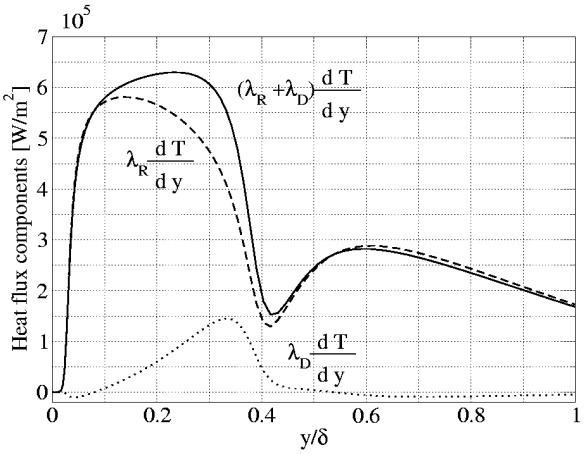


(b) **Heat ux components ($\lambda_R \nabla T$, $\lambda_D \nabla T$) along the stagnation line.**

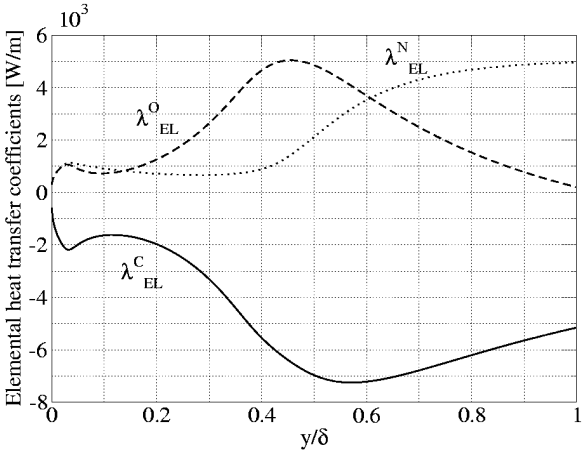


(c) **Elemental heat transfer coefficients.**

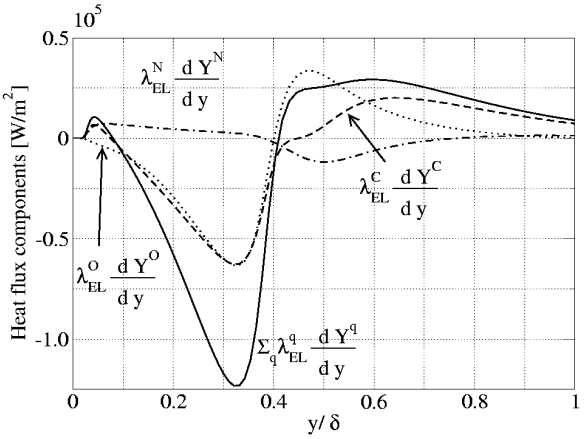


(d) **Heat ux components ($\lambda^q_{EL} \nabla Y^q$).**

Figure 7: Heat ux components, thermal conductivities, and elemental heat transfer coefficients.

coefficients presented in Fig. 7(a) helps us understanding the behavior of the various heat ux contributions. Indeed, the non-linear behavior of $\mathbf{q}_c$ can be easily explained. $\lambda$ is an increasing monotone function from the wall towards the outer edge, while $\partial T/\partial y$ starting from the outer edge increases, decreases and then increases again as shown in Fig. 3(a). Therefore $\mathbf{q}_c$ follows mainly the evolution of $\partial T/\partial y$. For what concerns $\mathbf{q}_d$, we need to consider separately the ve contributions $-\lambda_R \nabla T$, $-\lambda_D \nabla T$, and $-\lambda^q_{EL} \nabla Y^q$.
In Fig. 7(b), we present the evolution of the rst two terms and their sum. The evolution of these two contributions is more complex than the previous one since the two associated transport coefficients present a highly non-linear behavior with extrema in different positions than the temperature gradient. As far as the elemental heat transfer coefficients are concerned, we present their evolution in Fig. 7(c). There we notice that they all have a non-monotone behavior re ecting the highly reacting character of the o w. These transport coefficients lead to three contributions to the heat ux presented in Fig. 7(d), which are of the same order of magnitude for the three elements. The sum of these contributions is also plotted in the same gure to show the importance of

this term with respect to the total heat ux.
From the analysis of the pro les presented in Figs. 7(b)-7(d), we can justify the evolution of $\mathbf{q}_d$ concurring to the determination of the nal shape of the heat ux. As a nal step we analyze in detail the relative importance of the various terms contributing to the heat ux. In Fig. 8, we present the results of this analysis showing the evolution of the four following ratios along the stagnation line : $-(\lambda dT/dy)/q$, $-(\lambda_R dT/dy)/q$, $-(\lambda_D dT/dy)/q$, and $-(\sum \lambda_{EL}^q dY^q/dy)/q$.

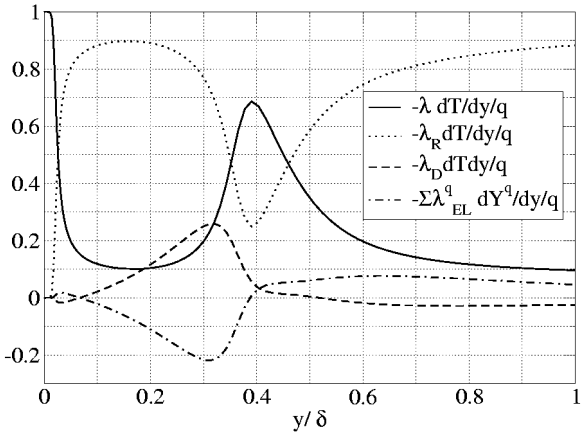


Figure 8: Normalized heat ux components.

The analysis of these pro les help us to quantify the importance of each term. Indeed, this shows that the major contribution to the heat ux comes from the thermal reactive conductivity ($\lambda_R$), the second comes from conduction ($\lambda$) and the two remaining contributions are of the same order of magnitude. The analysis of the curve $-(\lambda_D dT/dy)/q$ reveals that the contribution related to elemental demixing is higher than the one due to thermal conductivity for $0.1 < y/\delta < 0.3$. The two contributions $-\lambda_D dT/dy$ and $-\sum \lambda_{EL}^q dY^q/dy$ present almost an opposite behavior for $y/\delta < 0.4$. On the other hand, for $y/\delta > 0.4$ we notice that $-\sum \lambda_{EL}^q dY^q/dy$ becomes higher than $-\lambda_D dT/dy$ approaching the 10% of the total heat ux around $y/\delta \sim 0.6$ and decreasing to 5% at the outer edge. The almost opposite behavior of the two latter contributions clearly shows that elemental diffusive ux es have not a very important in uence on the total heat ux. Indeed if $\mathcal{J}_e = 0 \ \forall e \in \mathcal{E}$, the Butler and Brokaw thermal reactive conductivity is enough to compute $\mathbf{q}_d$. For the conditions previously analyzed, the presence of non vanishing elemental ux es acts on the mixture energetic behavior with a heat ux contribution which is at most of the order of 5% of the total heat ux.

# 4 Applications to ICP o w computation

In this section we present a detailed analysis of chemical equilibrium and non equilibrium plasma o ws both in the torch and in the test chamber. In the remaining part of the section we limit our discussion to the presentation of the results of several plasma o w simulations and we refer the interested reader to previous publications [64, 75, 17] for the description of the ICP model used to obtain these results. In the same references the reader will nd an extensive description of the models used to compute the thermodynamic and transport properties

of reacting mixtures such as those used to obtain the results to be presented shortly.
In Sec. 4.1 we will present results concerning only the torch domain for carbon dioxide plasmas, while in Sec. 4.2 we extend our investigation to the hot air jet flowing into the chamber.
The two following mixtures will be considered in this section to simulate air and carbon dioxide plasmas :

**Air-11 species :** $\tilde{\mathcal{E}} = \{O, N, e^+\}, \tilde{\mathcal{R}} = \{O_2, N_2, NO, NO^+, O^+, N^+, O_2^+, N_2^+\}$, and $\tilde{\mathcal{S}} = \tilde{\mathcal{R}} \cup \tilde{\mathcal{E}}$,

$CO_2$**-8 species :** $\tilde{\mathcal{E}} = \{O, C, e^+\}, \tilde{\mathcal{R}} = \{CO_2, O_2, CO, O^+, C^+\}$, and $\tilde{\mathcal{S}} = \tilde{\mathcal{R}} \cup \tilde{\mathcal{E}}$.

The analysis presented in the first part of this section is based on the study presented by Rini et al. in Ref. [65] where a code-to-code validation is presented for carbon dioxide plasmas in the VKI plasmatron torch. To this end the authors present the results of the simulation of $CO_2$ plasma flows within the VKI plasmatron torch carried out obtained independently from the two groups with the VKI-ICP and the IPM-$\alpha$ codes. The results of this comparison showed how the 1-D approach of the $\alpha$ code fails in the description of the Electric field within the torch. In addition, the importance of elemental diffusion on the behavior of $CO_2$ plasma flows is assessed and only this part will be presented in the following whose motivation is recalled hereafter:

(1) accurate carbon dioxide plasma flow simulations are rare in the literature related to aerospace sciences. Moreover, up to the best author knowledge, no simulation is available where elemental demixing is considered under thermochemical equilibrium conditions. For this reason we investigate the phenomena of elemental diffusion in LTE carbon dioxide plasmas to evaluate its effects on the flow behavior.

The second section is devoted to the physico-chemical characterization of the jet flowing in the test chamber for air plasmas, whose motivation is twofold :

(1) the methodology proposed by IPM [35] to estimate the catalytic properties of thermal protection system materials supposes thermochemical equilibrium conditions to be established in the torch and in the test chamber. However, there is no proof that equilibrium conditions exist and a detailed analysis assessing the quality of this assumption is not available. To supply this need we present both chemical non equilibrium and chemical equilibrium computations to provide a range of pressure in which equilibrium computations are as accurate as those obtained under chemical non equilibrium, using two finite rate chemistry models.

(2) As a result, we will be able to assess the influence of the finite rate chemistry model and operating pressure on the flow behavior both in the torch and especially in the test chamber.

## 4.1 Analysis of carbon dioxide plasma flows within the torch

We now move to the analysis of the numerical results obtained for an operating condition of the VKI plasmatron representative of Mars entry [33]. The analysis presented in this section is inspired on the study conducted by Rini et al. in Ref [65], omitting the part concerning the code-to-code comparison. Therefore, in the following,

we only present the investigation of elemental diffusion to assess the importance of the variations in carbon and oxygen elemental concentrations on the flow behavior. In Tab. 2, we present the operating condition selected as representative of Mars entry [33] used to produce the results to be presented shortly.

Table 2: Operating conditions for the VKI-Plasmatron operating with carbon dioxide.

| | |
|---|---|
| Ambient and wall temperature [K] | 300 |
| Power injected into the plasma [kW] | 90 |
| Frequency [MHz] | 0.37 |
| Inlet Swirl [deg] | 0 |
| Mass flow [g/s] | 8 |
| Operating pressure [Pa] | 7000 |

The flow has been simulated under LTE with both constant and variable elemental fractions and both computations have been carried out on the same mesh of 102 by 92 cells for which grid convergence is assured (Ref. [64]). All results presented in the following are converged at least 10 order of magnitude (based on the drop of the $L^2$ residual norm).

To investigate the influence of the elemental fraction variation on the flow behavior, we used the upgraded version of the VKI-ICP code [57] to simulate both the LTE-VEF and the LTE with Constant Elemental Fraction (LTE-CEF) formalisms. For that purpose, the plasma in the torch has been considered both under LTE-VEF and LTE-CEF conditions. For the operating conditions presented in Tab. 2 we obtain the elemental distribution presented in Fig. 9(a) in terms of carbon elemental mole fraction ($X^C$).

In Fig. 9(b), we present the temperature contours and in Fig. 9(c) the flow pattern, both within the torch, obtained under LTE-VEF conditions. In these figures, we observe the presence of a quite wide high-temperature region where the maximum temperature is around $\sim$ 10 000 K, as expected for the specified power injected in the flow. The mixture enters the torch with a reference elemental composition of 2/3-1/3 for oxygen and carbon respectively. Entering the torch, the mixture is subject to very strong temperature gradients which produce a non zero demixing contribution ($-\rho D_e^T \nabla T$) to the elemental diffusion flux [62], inducing elemental composition variations. Once a non-uniform elemental composition field is established, a counteracting mixing term ($\sum \rho D_{ck} \nabla Y^k$), proportional to the elemental composition gradients, tends to re-establish a uniform elemental field. These two mechanisms act together with convection to provide the final steady elemental composition pattern. From the analysis of Fig. 9(a), at least three zones can be observed. The first one represents an almost cylindrical zone delimited by $7.5 < r < 8.0$ cm close to the inlet and $6.0 < r < 8.0$ cm at the outlet. There, we do not observe substantial variations in the elemental fraction and this is mainly due to the fact that, in that region, the flow is continuously filled by a stream coming from the inlet with the reference elemental composition. In addition, the wall temperature being fixed, the axial temperature gradient is negligible close to the wall leading to the absence of diffusion in the same direction.

A second zone is visible around the torch axis both inside and after the recirculation bubble. There, we observe that carbon has the tendency to diffuse out from hot regions towards lower temperatures, leading to an axial zone poorer in carbon than in the case where a constant elemental composition is arbitrarily imposed. A third region is visible at the intermediate radii and a bit downstream of the inlet. There, the carbon mole fraction reaches the maximum value of 0.38, i.e. $\sim$ 13% more than the inlet value. This zone of high carbon concentration is therefore the result of the diffusion of carbon from the high temperature region around the axis accompanied by the difficulty for carbon to diffuse towards the quartz tube where the concentration is mainly

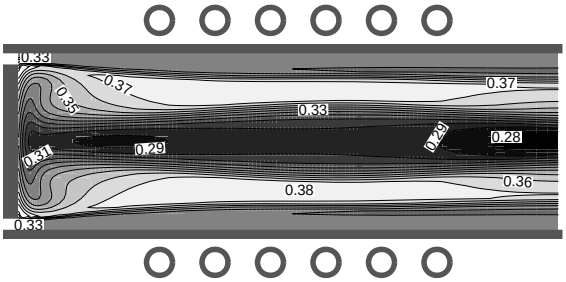


(a) **Carbon elemental molar fraction.**

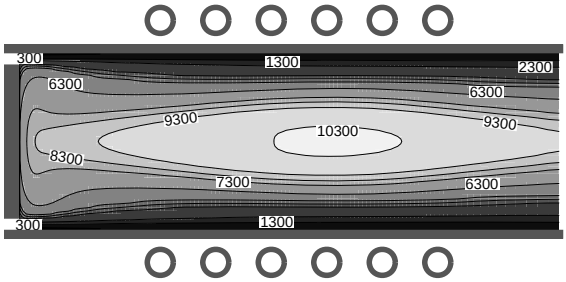


(b) **Temperature (K).**

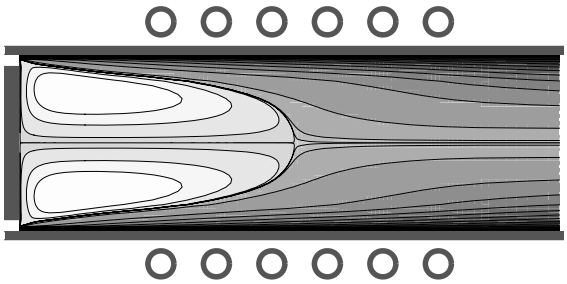

(c) **Stream function.**

Figure 9: Carbon dioxide plasma flows within the torch (LTE-VEF regime).

fixed by the cold mixture convected from the inlet to the torch exit.
The previous description of the carbon elemental field is reflected by the profile depicted in Fig. 10(a) which corresponds to the torch exit. There we clearly see that the carbon profile has a non-monotone behavior. As we approach the exit, the flow field became almost axial and radial convection can be neglected as shown in Fig. 9(c). This behavior of the outlet carbon elemental fraction, observed for nitrogen in air mixtures [64], could be predicted by observing the evolution of the elemental diffusion coefficients for the carbon element [59] as a function of temperature. In Figs. 10(b) and 10(c), we present the influence of elemental fraction variations on the mixture composition and on the mixture temperature. From the analysis of Fig. 10(b), a big influence of elemental fraction variations on the species concentration is observed. Starting from the wall we observe that, since the carbon molar fraction is slightly smaller than $1/3$, a small amount of $O_2$ is present close to the wall as a result of a LTE-VEF computation. Moving further towards the axis the differences between the CEF and the VEF computations become more evident. Indeed, the decrease of $X^C$ up to a local minimum around 6 cm causes a slower $CO_2$ dissociation accompanied by the displacement to lower radii of both the $O_2$ and the CO peaks. Then, because of the successive CO dissociation we observe the formation of both atomic carbon and oxygen, where the second one is more affected by the elemental fraction variation because of the retardation of both $O_2$ and CO peaks. Finally, atomic species decrease their concentration close to the axis because of ionization due to the high temperature around 10000 K. On the axis we therefore find a carbon fraction of $\sim 0.275$,

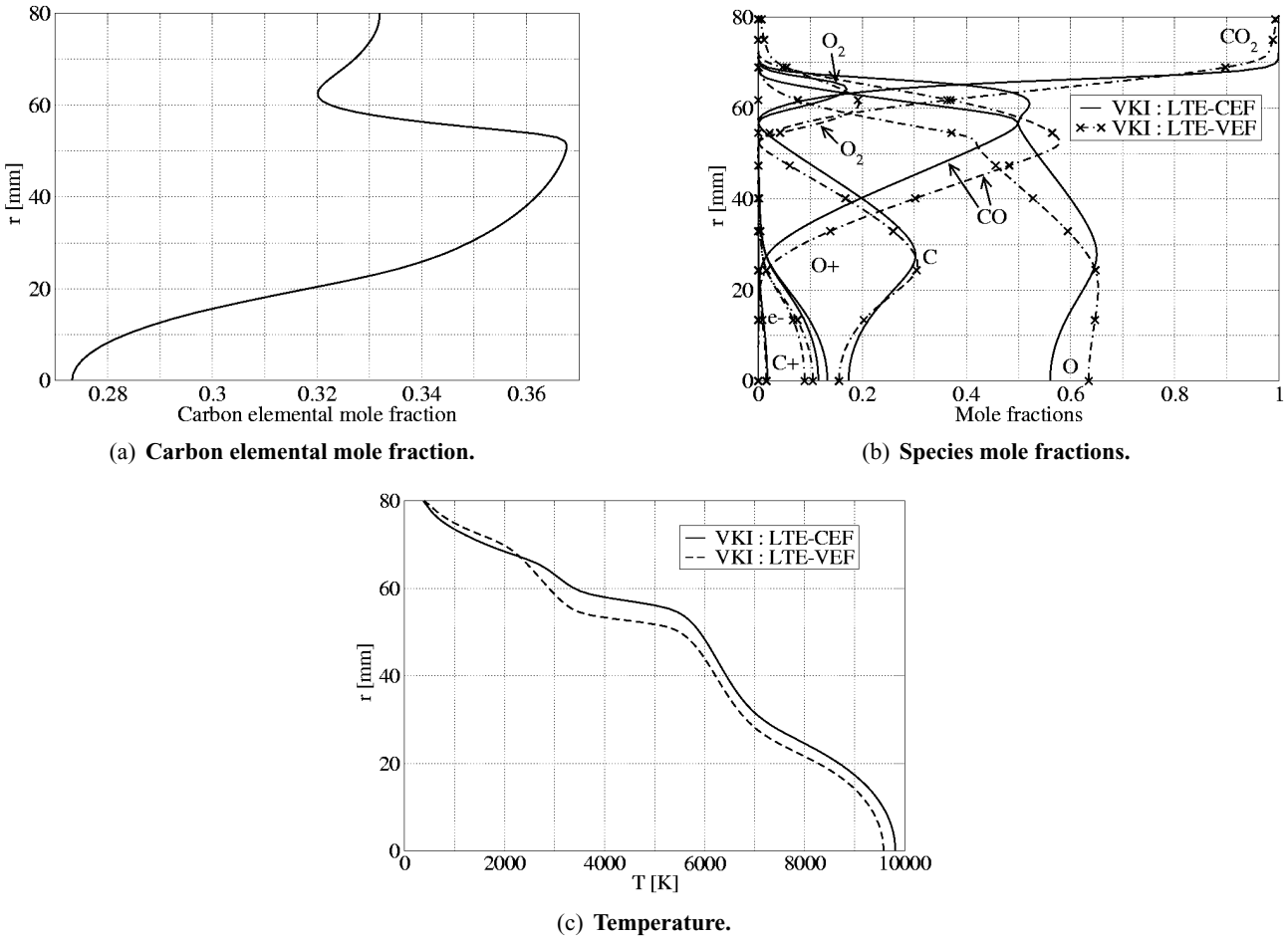


(a) **Carbon elemental mole fraction.**

(b) **Species mole fractions.**

(c) **Temperature.**

Figure 10: Radial pro les at the outlet of the torch.

i.e. ∼ 16% less than the reference value.
The nal in uence of elemental demixing is observed in Fig. 10(c), where the outlet temperature pro les for both CEF and VEF are compared. We notice the temperature to be overestimated in the case of constant elemental composition starting from $r < 7$ cm. By comparing Fig. 10(c) with the results presented in Ref. [64], we easily realize that the in uence of elemental diffusion on the temperature pro le is much higher for $CO_2$ than for air mixtures.

## 4.2 Characterization of air plasma o w in the test chamber

We now move to the analysis of air plasma o ws. The results to be presented shortly concern both the investigation of the torch and the hot exhaust jet in the chamber. As discussed at the beginning of this section, the forthcoming results will allow to verify for which operating conditions of the VKI plasmatron, the numerical simulation of LTE plasma o ws is as accurate as the chemical non equilibrium one, both in the torch

and especially in the test chamber. The consequences of this nding will have a direct impact on the range of applicability of the methodology used for the estimation of catalytic properties of thermal protection system materials [35].
The mesh used for the solution of the o w eld equations is divided into two blocks: the rst one (60 by 44 cells) is used to discretize the domain within the torch, while the second block (60 by 67 cells) reproduces a part of the test chamber. All results presented in the following are converged at least 10 order of magnitude (based on the drop in the $L_2$ residual norm).
The operating conditions, selected as representative of Earth (re)entry [51], are recalled in Tab. 3.

Table 3: Plasmatron operating conditions.

| | |
|---|---|
| Ambient and wall temperature [K] | 350 |
| Power injected into the plasma [kW] | 80 |
| Frequency [MHz] | 0.37 |
| Inlet Swirl [deg] | 0 |
| Mass o w [g/s] | 8 |
| Operating pressures [kPa] | 5, 10, 20, 30 |

For each simulation, the three chemical regimes chemical non equilibrium (CNEQ), LTE-CEF, and LTE-VEF have been considered.
In the following we present a qualitative analysis based on the investigation of the contour plots of the main o w properties and we refer the interested reader to Ref. [57] for a more detailed description of the o w behavior based on the analysis of temperature and elemental molar fraction pro les extracted in several crucial parts of the computational domain.
We rstly address the issue of the in uence of nite rate chemistry on the results of the simulation. To this end, two models have been selected as representative of Earth's atmosphere chemistry (Park [53] and Dunn-Kang [29]). Several numerical experiments have been conducted to assess how the operating pressure drives the o w behavior when one of the two models is used. As a result, we notice that the in uence of the nite rate chemistry is only limited to low pressures (around 5000 Pa). Indeed, as the operating pressure is set to higher values, the results obtained under CNEQ with both models are in very good agreement.
We start presenting temperature and elements concentration both in the torch and in the chamber by means of contour plots. Two of the four operating pressures speci ed in Tab. 3 have been selected to perform this study, the lowest (5000 Pa) and the highest (30000 Pa).
Focusing on these two pressures, we will be able to easily show how the differences observed in the o w solution, due to differences in the reaction rates, are visible only in the low pressure case and disappear when the operating pressure is increased up to 30000 Pa. The results to be presented shortly have been obtained under LTE-VEF conditions and under CNEQ using two nite rate chemistry models: the Park model [53], indicated as CNEQ-P, and the Dunn-Kang model [29] named as CNEQ-D&K.
Each non equilibrium result is compared with the respective one obtained with the other nite rate model but also with the result of the simulation carried out under thermochemical equilibrium with variable elemental fraction. This, at the same time, allows for the assessment of the in uence of the nite rate chemistry model and to answer the question of whether or not equilibrium computations give the same results as non equilibrium simulations for high pressures in the chamber.
In Figs. 11(a) and 11(b) we plot the temperature, respectively the oxygen elemental mass fraction both in the

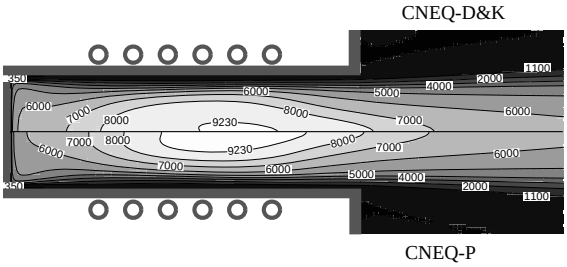


(a) **Temperature (K) contours obtained with two nite rate models.**

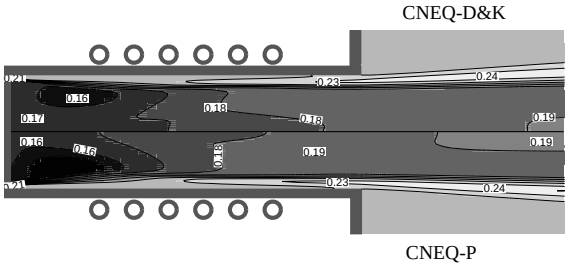


(b) **Oxygen elemental molar fraction obtained with two nite rate models.**

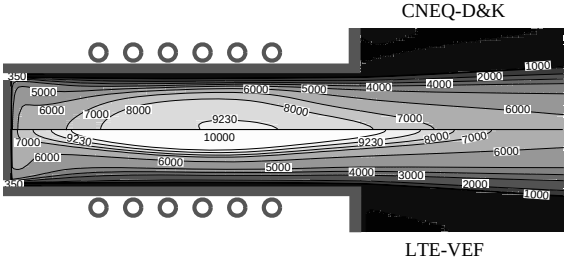


(c) **Comparison of the temperature (K) contours obtained with the Dunn-Kang model (upper) and under LTE-VEF (lower).**

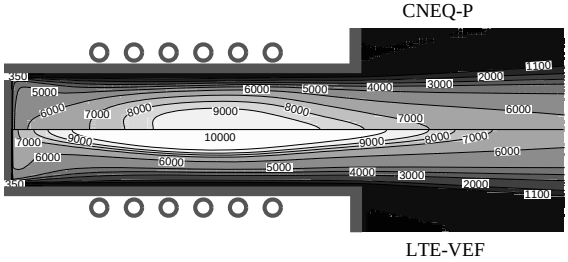


(d) **Comparison of the temperature (K) contours obtained with the Park model (upper) and under LTE-VEF (lower).**

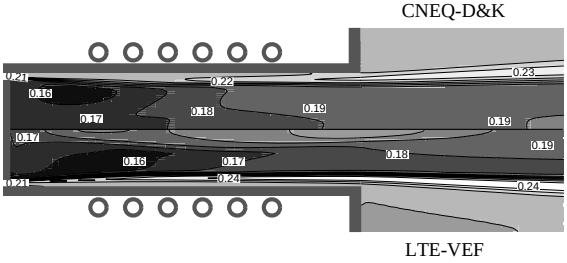


(e) **Comparison of the oxygen elemental molar fraction contours obtained with the Dunn-Kang model (upper) and under LTE-VEF (lower).**

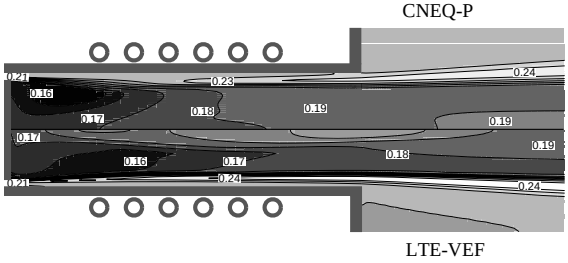


(f) **Comparison of the oxygen elemental molar fraction contours obtained with the Park model (upper) and under LTE-VEF (lower).**

Figure 11: Air plasma ow within the VKI plasmatron facility under CNEQ, LTE-CEF, and LTE-VEF conditions (5000 Pa).

torch and in the chamber. The analysis of these gures reveals the presence of two zones in which the comparison of the results bring us to different conclusions. Indeed, within the torch, we notice that the CNEQ-P and CNEQ-D&P predictions differ considerably leading to different temperatures and, to a lesser extent, elemental fractions. From Fig. 11(a) we observe that the Dunn-Kang model predicts a slightly wider hot (T≥ 6000 K) region in the torch acting on the structure of the plasma ball. As soon as we move towards the torch exit, we start noticing a rapid dwindling of the disparity between the two predictions which, at least from a qualitative point of view, show the same temperature eld in the jet, corresponding to the most interesting part of the

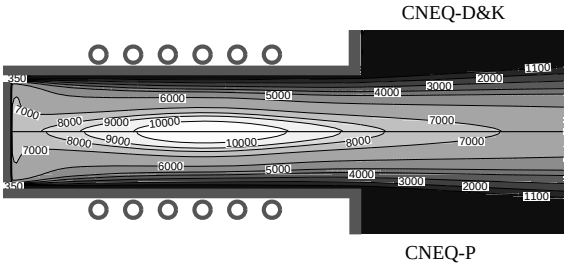


(a) **Temperature (K) contours obtained with two nite rate models.**

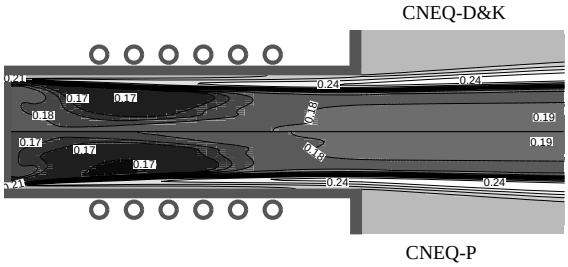


(b) **Oxygen elemental molar fraction obtained with two nite rate models.**

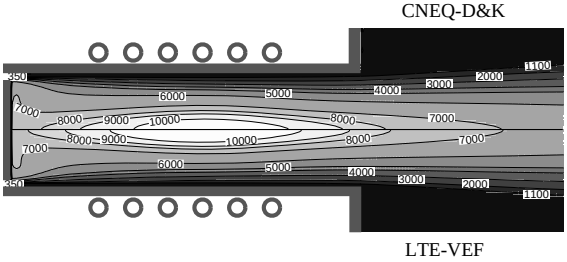


(c) **Comparison of the temperature (K) contours obtained with the Dunn-Kang model (upper) and under LTE-VEF (lower).**

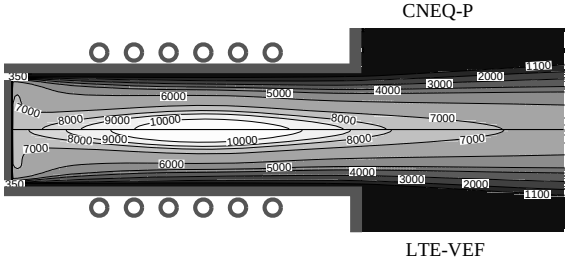


(d) **Comparison of the temperature (K) contours obtained with the Park model (upper) and under LTE-VEF (lower).**

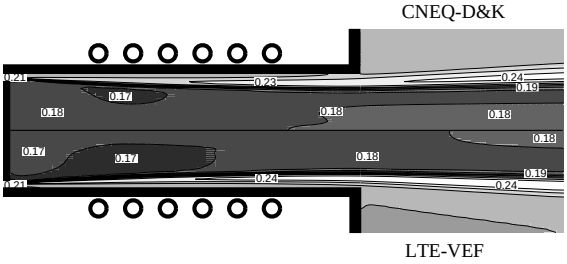


(e) **Comparison of the oxygen elemental molar fraction obtained with the Dunn-Kang model (upper) and under LTE-VEF (lower).**

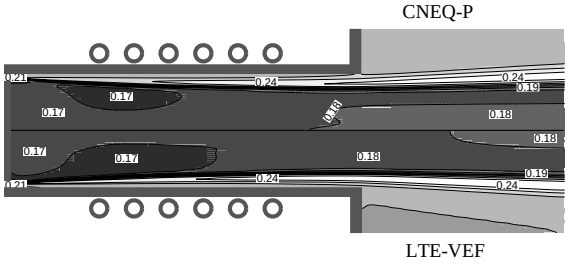


(f) **Comparison of the oxygen elemental molar fraction obtained with the Park model (upper) and under LTE-VEF (lower).**

Figure 12: Air plasma o w within the VKI plasmatron facility under CNEQ, LTE-CEF, and LTE-VEF conditions (30000 Pa).

o w eld from the point of view of TPM testing.

For what concerns the oxygen elemental fraction, we notice that the nite rate chemistry model has little in- uence on the elements concentration eld, showing once again that demixing is not a non equilibrium effect [Fig. 11(b)]. In Figs. 11(c)-11(d) and 11(e)-11(f), we present a comparison between the results obtained under chemical non equilibrium with the Park and Dunn-Kang models with those obtained under chemical equilibrium with variable elemental fractions. In Figs. 11(c)-11(d) we focus on the temperature contours while in Figs. 11(e)-11(f), we investigate the oxygen elemental fraction. As expected [64], the temperature contours ob-

tained under chemical non equilibrium differ considerably from those obtained with the equilibrium formalism and this for both nite rate chemistry models. From the oxygen elemental fraction presented in Figs. 11(e)-11(f) we notice a certain difference in the prediction of the elemental concentration eld between equilibrium and non equilibrium even though the order of magnitude of the oxygen variations is the same.
We now move to the analysis of the higher pressure (30000 Pa) and we start our analysis presenting, as done for the lower pressure case, the comparison between non equilibrium results. In Figs. 12(a)-12(b) we present the temperature, respectively the elemental fraction contours both in the torch and in the chamber. From the analysis of the temperature contours, we notice that at an operating pressure of 30000 Pa, the results obtained with the two models are, at least from a qualitative point of view, equivalent. The same conclusion is drawn after inspection of Fig. 12(b) where attention is focused on the oxygen elemental fraction. Differences between the prediction with the Park and the Dunn-Kang models are hardly visible. In the following, we present the comparison between the previous results with the respective equilibrium computations. The critical analysis of these comparison will enhance the importance of the previous conclusions. In Figs. 12(c)-12(d) and 12(e)-12(f) we present the direct comparison between the temperature, respectively the elemental mole fraction contours obtained both under chemical non equilibrium and equilibrium with variable elemental fraction. From Figs. 12(c)-12(d) we realize that the temperature contours predicted by the simulation of equilibrium conditions coincide with those obtained under chemical non equilibrium for both nite rate chemistry models after the last coil. Indeed, some small differences are visible within the torch until the last coil is reached. To further decrease these differences in the torch we just need to increase the operating pressure. On the other hand, at the torch exit, but most importantly in the test chamber, a perfect match is observed. Similar conclusions can be drawn for the elemental composition after inspection of Figs. 12(e)-12(f).
The results just described have a direct impact on the methodology used for the estimation of the catalytic properties of thermal protection materials. Indeed, thanks to the previous analysis we can argue that for sufficiently high pressures the equilibrium formalism allows for the determination of results, both in the torch and in the chamber, characterized by an accuracy very close to the one we can achieve with non equilibrium simulations. This conclusion will allow researchers performing inductively coupled plasma o w simulations for the characterization of TPM, to obtain accurate results using an equilibrium formulation at a fraction of the cost required to simulate the same conditions under non equilibrium.

# 5 Practical application to TPM testing

The von Karman Institute has been involved since 1997 in the determination of catalytic properties of thermal protection-system materials. Recently, with the initiation of several Mars exploration projects, interest has been attracted to Mars entry problems [19, 20, 11]. The two inductively coupled plasma (ICP) facilities of the Institute have been equipped to work with $CO_2$ mixtures [59]. The VKI high-enthalpy o w solvers are interfaced with libraries to compute thermodynamic, transport, and non equilibrium chemistry properties. The thermodynamic and transport libraries have been recently updated to incorporate $CO_2$ mixtures. In this section the physico-chemical description of a $CO_2$ o w is completed, allowing for simulations in chemical non equilibrium, characterized by both bulk and surface reactions. A critical output of the LHTS methodology is the heat load on the stagnation point of a ying body, where large gradients of temperature and mass concentrations are present. These features make this point a suitable benchmark for testing thermochemical models. The o w eld

in the vicinity of the stagnation point has been analyzed by means of stagnation-line flow calculations. These computations are applied for the determination of surface catalytic efficiency in $CO_2$ mixtures, leading to the determination of so-called heat-flux maps. The analysis that ensues is based on the study presented by Rini et al. in Ref. [59] whose motivation is recalled here after :

(1) the simulation of gas/surface interactions in $CO_2$ flows requires a special care because of the coupling between wall reactions sharing oxygen atoms. This is correctly described by the model presented by Rini et al. in Ref. [59], which will be successfully applied to describe heterogeneous recombination in carbon dioxide mixtures.

(2) The model proposed in Ref. [59] for the description of gas/surface interactions is compared against the one presented by Scott [69] showing that the latter one is not consistent with element mass conservation.

(3) In the aerospace related literature, the usual definition of a 'catalytic surface' is often given as the property of a certain material to promote recombination of atoms or molecules on the surface itself. As a consequence, a fully catalytic surface is said to be the one that forces a complete recombination inducing local conditions which tend to the equilibrium limit. Following this observation, several researchers working in the field of TPS design treat the gas/surface interactions for fully catalytic materials by computing the local mixture composition as the one corresponding to equilibrium conditions defined by the local pressure and temperature but using a reference elemental fraction, usually corresponding to the free stream. Thanks to the analysis of the results to be presented shortly, we will show that to define the equilibrium conditions representing the limit toward which a fully catalytic condition should tend, the local elemental fraction should be used instead of the free stream one.

(4) A crucial aspect of the methodology for the estimation of the catalytic properties of TPM is the heat flux map expressing the relation between wall heat flux, wall temperature and the effective recombination probability. As a final summary of the previous investigation, we will show how the outer edge elemental fraction affects the heat flux map. This will allow for the estimation of the influence that elemental demixing in the jet could have on the prediction of the effective recombination probability of thermal protection materials.

## 5.1 Stagnation line flow computations

In this section, we present the solution of the stagnation line differential problem for a carbon dioxide mixture under chemical non equilibrium conditions. As in Sec. 3, our attention will be focused mainly on the presentation of the results while we refer the interested reader to our previous publications [59, 4] for a complete description of the stagnation line equations. The test case definition is based on several simulations and experiments presented by Kolesnikov in Refs. [39] and [38] referring to the 100-kW IPG-4 plasmatron (IPM). Many calculations have been carried out at VKI [56] covering a wide range of enthalpy conditions. To investigate the importance of bulk and surface chemistry, we focus our attention on two operating conditions characterized by different outer edge enthalpies presented in Tab. 4, where $h_\delta$ is the mixture enthalpy at the outer edge, $V_s$ the incoming flow velocity and $p$ the operating pressure. This will lead to different chemical compositions and temperatures at the outer edge. As a consequence, different chemical processes will be enhanced by the

bulk recombination and the presence of atomic carbon at the outer edge in the second case, will in uence the de nition of the set of wall reactions.

Table 4: Flow conditions.

| | Low enthalpy case | High enthalpy case |
|---|---|---|
| $h_\delta$ [MJ/kg] | 15.3 | 39 |
| $p_\delta$ [atm] | $5.8{\cdot}10^{-2}$ | 0.1 |
| $R_m$ [mm] | 25 | 25 |
| $\delta$ [mm] | 10 | 10 |
| $v_\delta \partial/\partial y(\partial u_\delta/\partial x)/(\partial u_\delta/\partial x)^2$ [-] | 2.09 | 2.09 |
| $\partial u_\delta/\partial x$ [$s^{-1}$] | 1794 | 2558 |

The o w is considered to be under equilibrium conditions at the boundary layer edge. Therefore, the outer edge temperature is the result of an iterative calculation in which the thermodynamic modeling of the o w plays an important role. The corresponding values of temperature are 5922 K and 8127 K for the low and high enthalpy cases respectively.

Table 5: Chemical reactions used in the Stagnation Line computations. (M=$CO_2$, CO, $O_2$, O, C)

| *Dissociation reactions* |
|---|
| $CO_2 + M \rightleftarrows CO + O + M$ |
| $CO + M \rightleftarrows C + O + M$ |
| $O_2 + M \rightleftarrows O + O + M$ |
| *Neutral exchange reactions* |
| $CO+O \rightleftarrows C+O_2$ |
| $CO_2+O \rightleftarrows CO+O_2$ |

For the given o w conditions at the boundary layer edge, the heat ux at the stagnation point of the model has been computed as a function of the surface temperature $T_w$ and the surface effective catalycity $\gamma_w$, from the solution of the stagnation line equations. The analysis of the non equilibrium dissociated subsonic o w around the model is based on the assumptions used to derive the stagnation line equations [4, 59] and the following ones :

- the gas is represented by a 5 species ($CO_2$,CO,$O_2$,O,C) viscous and heat conductive mixture.
- The reaction set describing the nite rate bulk chemistry of the o w is the one described in Tab. 5.
- The surface catalytic reactions proceed according to the Eley-Rideal mechanism [21] and the following models are considered for the various cases analyzed.

  **2-surface reactions model :**

  (1) $O + (O - S) \rightarrow O_2 + S$ (2) $CO + (O - S) \rightarrow CO_2 + S$

  **3-surface reactions model :**

  (1) $O + (O - S) \rightarrow O_2 + S$ (2) $CO + (O - S) \rightarrow CO_2 + S$ (3) $C + 2(O - S) \rightarrow CO_2 + 2S$

Another important assumption in the present model is that all the recombining species have the same effective recombination probability, i.e. for the mentioned wall chemistry model we have

$$\gamma_{COw} = \gamma_{Ow} = \gamma_{Cw} = \gamma_w. \tag{14}$$

As the result of the computations performed along the stagnation line, for a 50 mm diameter probe, several charts have been determined for the stagnation point heat ux as a function of $T_w$ and $\gamma_w \in [0, 1]$, and will be presented later in this section.

### 5.1.1 Gas surface interactions

The description of non equilibrium o ws requires the modeling of recombination phenomena happening at the solid surface. To this end we have speci ed two sets of heterogeneous reactions. The next step consists in modeling the way in which the species involved in these reactions exchange atoms in order to express the mass production term $\omega_{i,cat}$ as a function of known quantities. Scott [69] proposes a model of the boundary conditions for the species equations [Eq. (7)] based on the following expression for the net mass ux of species $i$ at the surface

$$\omega_{i,cat} = M_i \mathcal{M}_i^{\downarrow} \sum_{r=1}^{N_r} \nu_{ri} \gamma^r - \sum_{r=1}^{N_r} \sum_{j=1}^{N_{sp}} \mu_{ijr} \gamma^r M_j \mathcal{M}_j^{\downarrow}, \tag{15}$$

where $\gamma^r$ is the reaction probability of the $r^{th}$ reaction, $M_i$ the molar mass of the $i^{th}$ species, and $\mathcal{M}_i^{\downarrow}$ is the thermal agitation ux of $i$-particles towards the surface. The matrix $\nu_{ri}$ indicates which $i^{th}$ reactants collide upon the surface in the $r^{th}$ reaction, while the matrices $\mu_{ijr}$ de ne the $j^{th}$ incident reactants producing the $i^{th}$ products for the $r^{th}$ reaction. Within the methodology followed for the determination of catalytic properties of TPS materials, the reaction probability $\gamma^r$ is supposed to be independent from the reaction and equal to an effective recombination probability $\gamma_w$.
Therefore, the expression for the impinging ux $\mathcal{M}_i^{\downarrow}$, if the Chapman-Enskog perturbation term is considered, reads

$$\mathcal{M}_i^{\downarrow} = \frac{2}{2 - \gamma_w} n_i \sqrt{\frac{kT_w}{2\pi M_i}}.$$

This formulation ensures a zero net total mass ux at the wall but does not satisfy in general the element conservation, indeed, considering a catalytic surface model constituted by the two reactions $O + O \rightarrow O_2$ and $CO + O \rightarrow CO_2$, one notices a coupling between the two chemical processes. This in some way establishes a link between the reaction probabilities of the two reactions which is not speci ed in the previous formulation.
Elaborating further on this consideration, an alternative approach is proposed. Let us de ne a rate of reaction per unit surface and unit time for the wall reaction $\chi_k$, which represents the frequency at which reactions take place on the surface.
With this in mind, a formalism similar to the one used for bulk reactions is followed. The number of moles produced per unit surface and unit time are given by

$$\frac{\omega_i}{M_i} = \sum_{r=1}^{N_r} \left( \nu_{ir}'' - \nu_{ir}' \right) \chi_r \tag{16}$$

where, for $\nu'_{ir} \neq 0$

$$\chi_r = \gamma_i^r \frac{\mathcal{M}_i^{\downarrow}}{\nu'_{ir}}. \tag{17}$$

The surface reaction rate $\chi_r$ is therefore related to the recombination probability of species $i$ involved in the $r^{th}$ reaction $\gamma_i^r$ by the relation (17). As the reaction rate $\chi_r$ has to be independent of the species $i$, it results that the species reaction probabilities $\gamma_i^r$ are linked by the constraints $\gamma_i^r \mathcal{M}_i^{\downarrow}/\nu'_{ir} = \text{constant} = \chi_r$, for all species such that $\nu'_{ir} \neq 0$.
In this case, the ux of particle $\mathcal{M}_i^{\downarrow}$ is given by $\mathcal{M}_i^{\downarrow} = 2/(2-\gamma_i) n_i \sqrt{kT_w/(2\pi M_i)}$, while $\gamma_i = \sum_{r=1,N_r} \gamma_i^r$ represents the recombination probability of species $i$. The computation of the boundary condition for the species continuity equations will therefore consists in rstly calculate $\chi_r$ and then evaluating the production term by means of Eq. (16). The purpose of this alternative formulation is not to better describe the physical phenomenon of heterogeneous catalycity, which is hidden in the de nition of the different recombination probabilities. But at least, it provides a model which is consistent with both the global mass and element conservation at the wall, as will be demonstrated by numerical experiments. Moreover, it should be noticed that the quantity $\chi_r$ depends only on the reaction considered and not on the species involved in it, which represents another similitude with the bulk reaction mechanism.

### 5.1.2 Low enthalpy case

We start our analysis considering the low enthalpy case for which only the 2-surface reactions model has been applied, using both Scott's model [69] and the formulation presented in the previous section. This reaction scheme is based on the recombination of atomic oxygen and carbon oxide to produce molecular oxygen, respectively carbon dioxide. The success of these two processes is based on the simultaneous presence of O and CO close to the surface. The atomic oxygen will then concur to both recombination processes while CO only to one of them. The description of the kinetics of these two reactions requires the knowledge of the rates of each chemical process. These frequencies will be computed on the basis of the effective probability that an atom of oxygen has to be involved in the $i^{th}$ process ($\gamma_O^i$) and on the probability that a molecule of CO has to be involved in the $j^{th}$ reaction ($\gamma_{CO}^j$). Obviously these effective recombination probability are related by mass conservation and constrained by Eq. (14). Nevertheless, a correct treatment of these issues is missed in several gas/surface interaction models [69, 35], whereas they are correctly described by the formalism presented in Sec. 5.1.1 which in the present case reads :

$$\gamma_O^1 + \gamma_O^2 = \gamma_O, \quad \gamma_{CO}^2 = \gamma_{CO}, \quad \gamma_O^2 \mathcal{M}_O^{\downarrow} = \gamma_{CO}^2 \mathcal{M}_{CO}^{\downarrow}, \tag{18}$$

where, thanks to Eq. (14), $\gamma_O = \gamma_{CO} = \gamma_w$. Eqs. (18) constitute a $3 \times 3$ system in the unknowns $\gamma_O^1$, $\gamma_O^2$, $\gamma_{CO}^2$ which must also satisfy the inequalities $0 \leq \gamma_i^r \leq \gamma_w$. The solution is easily obtained

$$\gamma_{CO}^2 = \gamma_w, \quad \gamma_O^2 = \gamma_{CO}^2 \frac{\mathcal{M}_{CO}^{\downarrow}}{\mathcal{M}_O^{\downarrow}}, \quad \gamma_O^1 = \gamma_w - \gamma_O^2. \tag{19}$$

This solution is valid as long as $\gamma_O^2 \leq \gamma_w$. If it is not, then it means that one of the assumptions made does not hold (e.g. equal recombination probability for all species). In practice, $\gamma_O^2$ was always below $\gamma_w$ for our

computations. Then, the reaction frequencies [Eq. (17)] are obtained as

$$\chi_1 = \frac{\gamma_O^1 \mathcal{M}_O^{\downarrow}}{2}, \quad \chi_2 = \gamma_{CO}^2 \mathcal{M}_{CO}^{\downarrow}, \tag{20}$$

leading to the following expressions for the species production terms

$$\frac{\omega_{CO_2}}{M_{CO_2}} = \gamma_{CO}^2 \mathcal{M}_{CO}^{\downarrow}, \quad \frac{\omega_{CO}}{M_{CO}} = -\gamma_{CO}^2 \mathcal{M}_{CO}^{\downarrow}, \frac{\omega_{O_2}}{M_{O_2}} = \frac{\gamma_O^1 \mathcal{M}_O^{\downarrow}}{2}, \quad \frac{\omega_C}{M_C} = 0, \quad \frac{\omega_O}{M_O} = -(\gamma_O^1 + \gamma_O^2)\mathcal{M}_O^{\downarrow}. \tag{21}$$

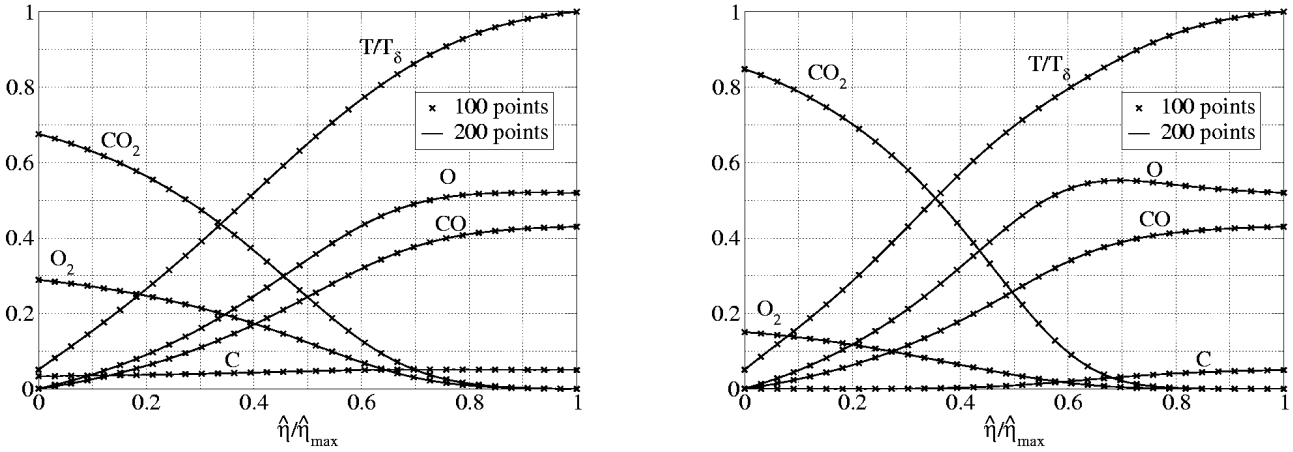


(a) **McKenzie bulk chemistry model.** (b) **Park bulk chemistry model.**

Figure 13: Species mass fraction and non dimensional temperature pro les [Surface reaction model presented in Eq. (21), $\boldsymbol{h_\delta}$=15.3MJ/kg, $\boldsymbol{T_w}$=300K], [0: wall; 1: $\boldsymbol{\delta}$].

We now move to the presentation of the solution of the stagnation line problem [59]. All the computations showed in the following are converged for a 100 points discretization of the stagnation line. A grid resolution study was conducted to obtain reliable heating predictions. Species mass fraction and non-dimensional temperature pro les along the stagnation line are shown in Fig. 13 for 100 and 200 equidistant point grids, for both the McKenzie [Fig. 13(a)] and Park [Fig. 13(b)] bulk chemistry models. The solutions for both mesh re nements are seen to be identical, showing the grid independence of the results. The analysis of Fig. 13 reveals a non negligible in uence of the bulk chemistry model. The main difference in the predictions obtained with the two sets of nite rate chemical processes lies in the evolution of atomic carbon along the stagnation line. The McKenzie model does not enhance considerably C recombination, while for the Park model C is involved in the formation of $CO_2$ starting from 80% of the stagnation line and it is completely depleted when we reach the 40% of the stagnation line. As a consequence, in Fig. 13(a) we observe that, even if CO disappears completely, a lower amount of $CO_2$ is present at the wall with respect to the computations obtained with the Park model. In addition, since less carbon is available for recombination, a higher amount of $O_2$ is observed at the wall for the prediction obtained with the McKenzie model. The difference in the prediction of atomic carbon chemistry will be more evident for the high enthalpy case and some of the previous observations will be helpful for the de nition of the set of wall reactions.

We now turn our attention to the analysis of the diffusion demixing phenomenon considering three different wall boundary conditions :

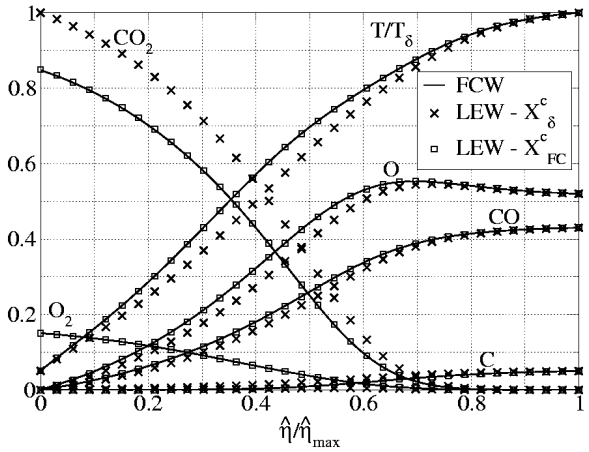


Figure 14: Mass fractions and non-dimensional temperature for three different boundary conditions (Park bulk chemistry model) [$\boldsymbol{h_\delta}$=15.3MJ/kg, $T_w$=300K].

- fully catalytic wall (present wall chemistry model - FCW);
- equilibrium wall with the element fraction of the outer edge (LEW - $X^c_\delta$);
- equilibrium wall with the element fraction corresponding the fully catalytic case (LEW - $X^c_{FC}$).

The wall heat ux corresponding to these cases is summarized in Tab. 6.

Table 6: Wall heat ux for several boundary conditions (Park chemistry model) [$\boldsymbol{h_\delta}$=15.3MJ/kg, $\boldsymbol{T_w}$=300K].

| Boundary Condition | $q_w[MW/m^2]$ |
|---|---|
| FCW | 0.856 |
| LEW - $X^c_{FC}$ | 0.857 |
| LEW - $X^c_\delta$ | 0.918 |

Assuming a local equilibrium wall with the outer edge elemental fraction results in an overestimation of the wall heat ux, which is explained as follows. The wall heat ux is primarily controlled by the recombination processes taking place at the wall. Due to diffusion demixing in the boundary layer, there is more oxygen and less carbon at the wall then at the outer edge (see Fig. 14 which shows the mass fraction pro les for the 3 boundary conditions). As a result, fewer $CO_2$ molecules can be formed, the excess oxygen forming $O_2$ molecules. Hence, less heat is released than if C and O elements were in the $1/3 - 2/3$ proportion.
These results point out the importance of diffusion demixing effects, in particular regarding their in uence on wall heat ux, and clearly establishes that the local equilibrium boundary condition based on outer edge (free stream) elemental fractions, widely used in the framework of hypersonic o ws simulations, is incorrect [61, 60].
At this point, it is interesting to comment on the relation between elemental diffusion and surface chemistry. Indeed, some approximate models used to describe stagnation line o ws are based on the constant elemental

fraction assumption as for example in the $\gamma$-code developed at IPM [36]. Under chemical non equilibrium conditions, using the 2-surface reactions model, both $O_2$ and $CO_2$ should be present at the wall under fully catalytic conditions. On the other hand, if constant elemental fraction is assumed through the boundary layer, equal to the outer edge one (1/3-2/3), the co-presence of these two species is not possible. Indeed, as shown in Ref. [66], the results of the $\gamma$-code operating with $CO_2$ mixtures under non equilibrium and for a fully catalytic surface, based on the 2-surface reactions scheme, show the presence of only $CO_2$ on the surface for cold wall conditions. This is clearly in contradiction with the equal effective recombination probability which is one of the major assumption of the IPM methodology. We wish to stress that the model presented in Sec. 5.1.1 is free of these inconsistency.

Another illustration of the importance of the demixing phenomenon is provided by comparing Scott's and the present formulation for a fully catalytic wall. Computed elemental fraction pro les are presented in Fig. 15, always for the low enthalpy case. Elemental fractions of carbon ($X^C$) and oxygen ($X^O$) de ned in Eq. (5), are related to molar elemental concentration ($\xi_i$) as follows :

$$X^O = \frac{\xi_O}{\xi_C + \xi_O} \quad \text{and} \quad X^C = \frac{\xi_C}{\xi_C + \xi_O}$$

where

$$\xi_C = (x_{CO_2} + x_{CO} + x_C)\frac{p}{R_u T} \quad \text{and} \quad \xi_O = (2x_{CO_2} + x_{CO} + 2x_{O_2} + x_O)\frac{p}{R_u T}$$

$R_u$ being the universal gas constant. From the analysis of Fig. 15(a) we observe that for Scott's formulation $X^O > X^{O,\delta}$ throughout the boundary layer, which is in contradiction with the elemental balance [59]. Indeed, in general only convective ux es are signi cant in the elemental balance (the wall diffusion ux is zero and the edge diffusion ux is negligible) so that the elemental balance [59] reduces to

$$\xi_{j\delta} V_\delta + 2\frac{\partial u_\delta}{\partial x}\frac{\delta}{\int_0^{\hat{\eta}_{max}} \frac{d\hat{\eta}}{\rho}} \int_0^{\eta_{max}} \xi_j \frac{F(\hat{\eta})}{\rho} d\hat{\eta} = 0. \tag{22}$$

Hence, the elemental concentration ($\xi_j$) distribution must be such that some weighted average of it equals the outer edge concentration, and similarly for the elemental fraction ($X^j$), which is not veri ed when $X^O > X^{O,\delta}$ throughout the boundary layer. In contrast, the elemental fraction distributions obtained with the present wall chemistry model are compatible with this condition [Fig. 15(b)].

In fact, the elemental fraction distribution obtained with Scott's wall chemistry model violates this condition because this model does not respect elemental conservation at the wall. For the present problem, it provides a source of O and a sink of C at the wall. This was veri ed by computing the elemental diffusion ux es at the wall and observing that

$$C: \ \frac{J^y_{CO_2 w}}{M_{CO_2}} + \frac{J^y_{COw}}{M_{CO}} + \frac{J^y_{Cw}}{M_C} < 0 \qquad O: \ 2\frac{J^y_{CO_2 w}}{M_{CO_2}} + \frac{J^y_{COw}}{M_{CO}} + 2\frac{J^y_{O_2 w}}{M_{O_2}} + \frac{J^y_{Ow}}{M_O} > 0.$$

We now analyze the calculated heat ux maps for the present o w conditions. Heat ux maps consist of curves of wall heat ux ($q_w$) as a function of wall temperature between 300 K and 2100 K for various values of the recombination probability $\gamma_w$. Four different maps have been obtained for the present test case, corresponding to all possible bulk chemistry (Park/McKenzie) and wall chemistry (Scott/present) model combinations. They

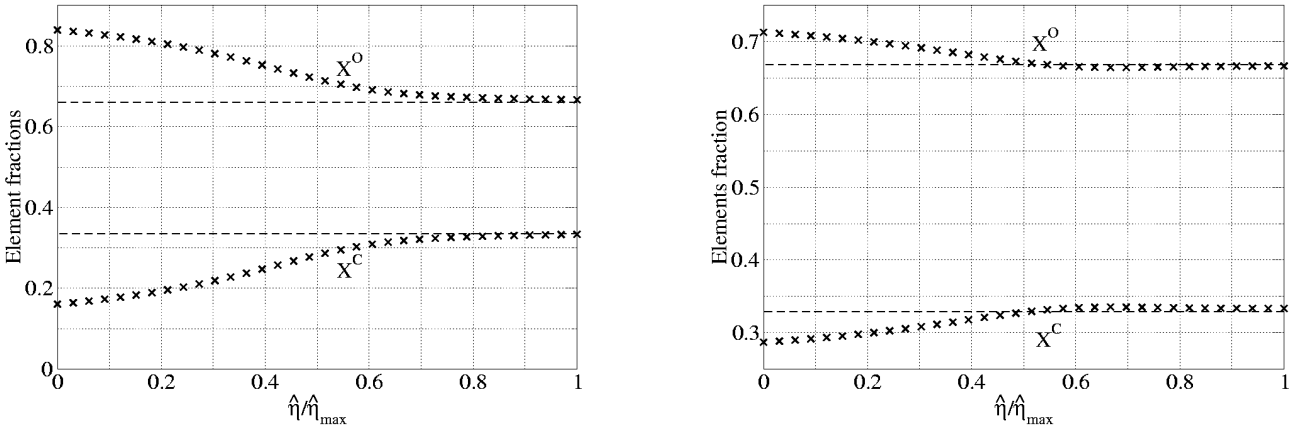


(a) **Scott wall chemistry model.** (b) **Present wall chemistry model.**

Figure 15: Element fractions computed with the Scott's and the present catalycity models (Park bulk chemistry model) [0: wall; 1: $\delta$].

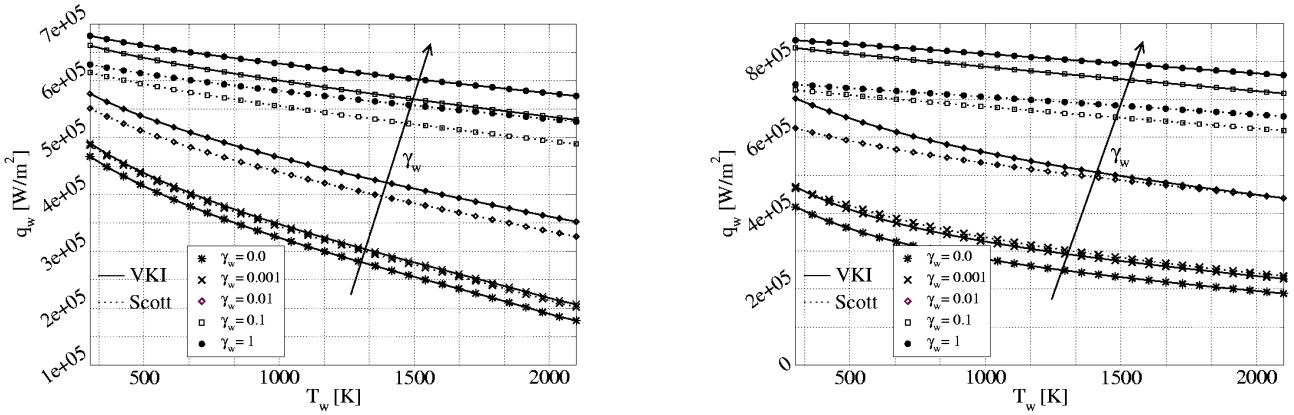


(a) **McKenzie bulk chemistry model.** (b) **Park bulk chemistry model.**

Figure 16: Heat ux maps for the lower enthalpy case [$h_\delta$=15.3MJ/kg].

are displayed in Fig. 16.

The in uence of the bulk chemistry model is clearly visible. Park's model reaction rates being much larger than McKenzie's, the wall heat ux is signi cantly larger for low wall temperatures and low recombination probabilities. The in uence of the wall reaction model is also important for large recombination probabilities. For high values of catalycity, the heat ux is seen to be signi cantly higher with the present model, which is consistent with the fact that, because of the existence of a sink of C atoms at the wall in Scott's model, there are fewer C atoms available for recombination.

### 5.1.3 High enthalpy case

Attention is now turned to the high enthalpy case. Because of the higher enthalpy level, the mass fraction of C atom at the outer edge is much higher, so that the third wall reaction, $C + 2(O - S) \rightarrow CO_2$, may become important. For this reason, we first analyze the influence of the wall reactions set using Scott's formulation for both bulk chemistry models. Species mass fractions and non-dimensional temperature profiles are shown in Fig. 17 for a fully catalytic wall. Whereas for Park's model there is no influence of the wall reactions set because the carbon atom entirely recombines inside the boundary layer (bulk chemistry), on the contrary the wall reactions set has a large influence when using McKenzie's model, for which bulk reactions are much slower.

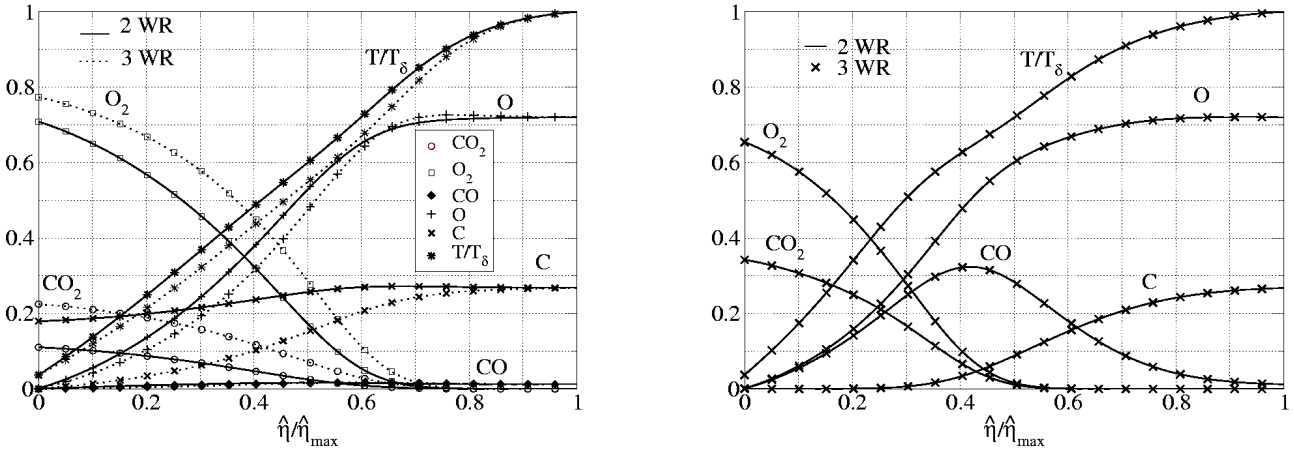


(a) **McKenzie bulk chemistry model.** (b) **Park bulk chemistry model.**

Figure 17: Mass fractions and non-dimensional temperature profile [$h_\delta$=39MJ/kg, $T_w$=300K][0: wall; 1: $\delta$].

In particular, if the third wall reaction is ignored, there remains an important amount of atomic carbon at the wall. As a result, the wall heat flux is considerably smaller (see Tab. 7 in which heat fluxes are listed for all bulk chemistry/wall reaction set combinations).

Table 7: Wall heat flux for several sets of surface reactions [$h_\delta$=39MJ/kg, $T_w$=300K].

| Surface | Stagnation Line | $q_w[MW/m^2]$ |
|---|---|---|
| Scott 2WR | McKenzie | 1.20 |
| Scott 3WR | McKenzie | 2.14 |
| Scott 3WR | Park | 2.23 |
| Scott 2WR | Park | 2.24 |

The present formulation for the 3 wall reactions model reads as follows

$$\gamma_O^1 + \gamma_O^2 + \gamma_O^3 = \gamma_O, \quad \gamma_{CO}^2 = \gamma_{CO}, \quad \gamma_C^3 = \gamma_C, \quad \gamma_O^2 \mathcal{M}_O^{\downarrow} = \gamma_{CO}^2 \mathcal{M}_{CO}^{\downarrow}, \quad \gamma_C^3 \mathcal{M}_C^{\downarrow} = \frac{\gamma_O^3 \mathcal{M}_O^{\downarrow}}{2}, \tag{23}$$

where $\gamma_{CO} = \gamma_O = \gamma_C = \gamma_w$. Eqs. (23) represent a system of 5 equations in 5 unknowns $\gamma_O^1$, $\gamma_O^2$, $\gamma_O^3$, $\gamma_{CO}^2$, and $\gamma_C^3$. For the present o w conditions, numerical experiments have shown that the solution does not satisfy the constraint $\gamma_O^3 \leq \gamma_w$, which implies that the hypothesis of equal recombination probabilities for all species does not hold [71]. The analysis of a suitable assumption is however left as an open subject for a further study.
We therefore switch our attention to the Park bulk chemistry/2 wall reaction model for the present high enthalpy case.

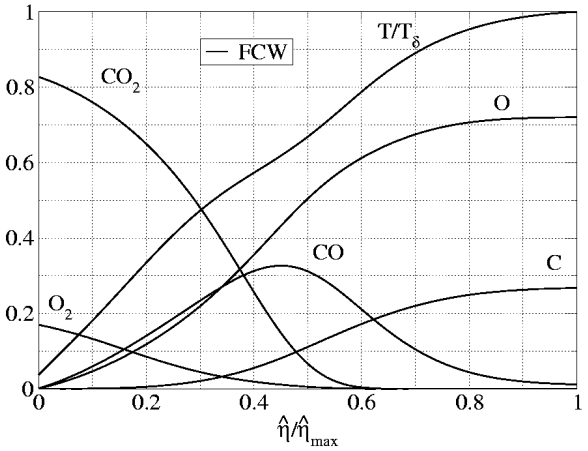


(a) **Mass fractions and non-dimensional temperature pro le. ($T_w$=300K) (0: wall; 1:$\delta$).**

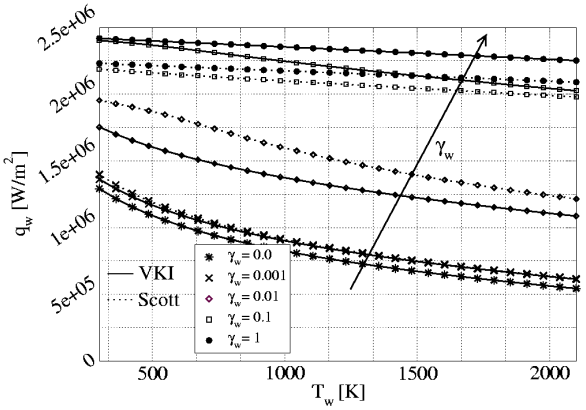


(b) **Heat ux map.**

Figure 18: Stagnation line solution for the higher enthalpy case (Park bulk chemistry model) [$\boldsymbol{h_\delta}$=39MJ/kg].

Species mass fraction and non-dimensional temperature pro les for a fully catalytic wall computed using the present wall chemistry formulation are shown in Fig. 18(a). This is to be compared with Fig. 17(b) where Scott's formulation was used. The same conclusion as for the low enthalpy case is obtained, i.e. for high $\gamma_w$ Scott's model acts as a sink of carbon atoms at the wall. As a result, the wall heat ux is smaller, as seen in Fig. 18(b) which shows the heat ux map for the high enthalpy case.

### 5.1.4 In uence of outer edge elemental fractions on heat ux maps

As discussed in the introduction, the methodology developed at the IPM and currently used at VKI to estimate the catalycity properties of TPS materials, is based upon Navier-Stokes simulations of an ICP facility supposed to be under LTE conditions determined assuming constant elemental fractions.
The purpose of the Navier-Stokes plasma o w simulation is to provide the LTE outer edge inputs for the nite thickness non equilibrium stagnation line o w computations, carried out to compute a heat ux map. Among the quantities needed, the composition is implicitly given as a function of the outer edge pressure and rebuilt-enthalpy, assuming LTE and using the torch inlet elemental fractions. In general, thanks to elements diffusion, the elemental fractions vary within the ICP facility [76], as shown in Sec. 4, leading to an outer edge elemental composition different from the torch inlet one. If this difference has an in uence on the heat ux map, by shifting or stretching the iso-catalycity lines, the same in uence will be re ected to the estimation of TPS material catalycity.

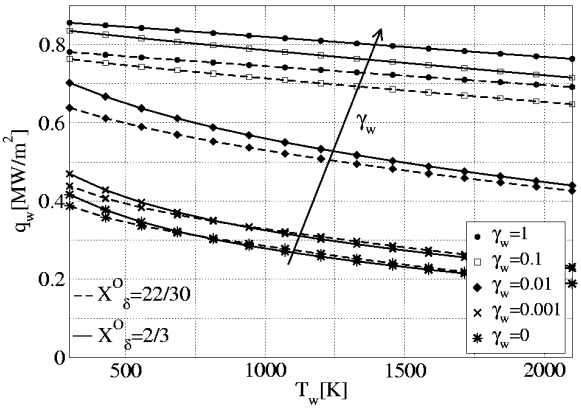


(a) **Heat ux map : $CO_2$ mixture.**

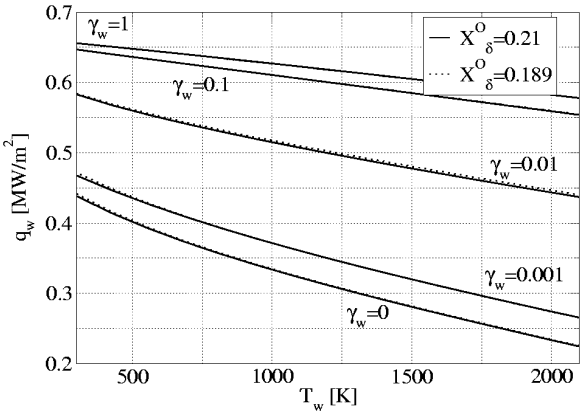


(b) **Heat ux map: air mixture.**

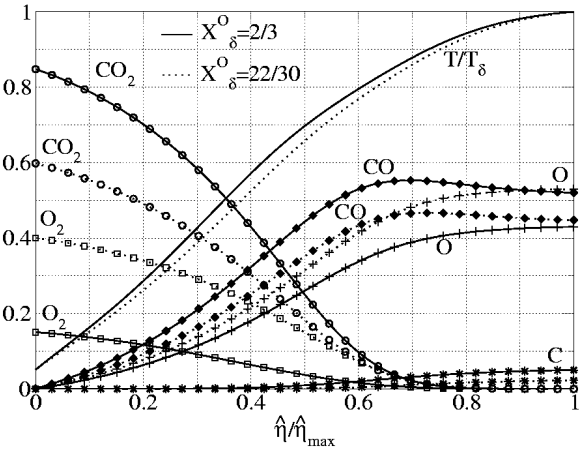


(c) **Species mass fraction :** $CO_2$ **mixture (**$T_w = 300K, \gamma_w = 1$**) (0:**$w$**;1:**$\delta$**)**

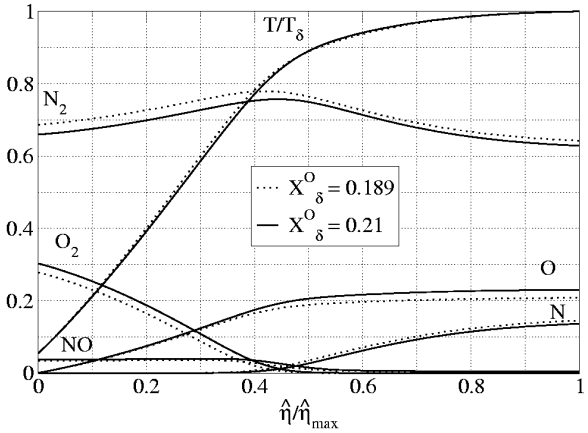


(d) **Species mass fraction : air mixture (**$T_w = 300K, \gamma_w = 1$**) (0:**$w$**;1:**$\delta$**)**

Figure 19: In uence of outer edge elemental fraction on the stagnation line solution [The outer edge conditions are speci ed in Ref. [58]].

One way to easily estimate this in uence is to use the results of the constant elemental fraction ICP simulation and vary only the outer edge elemental fractions, used to determine the outer edge composition for the given enthalpy and pressure. In Sec. 4 we found an oxygen elemental fraction lower than the inlet value ($X^O_\delta = 0.21$) in the jet near the axis for air plasmas. On the other hand, for carbon dioxide o ws the opposite behavior was observed, i.e. the oxygen elemental fraction reached values higher than at the torch inlet ($X^O_\delta = 2/3$). Following this result, we have perturbed the oxygen outer edge elemental fraction by $+10\%$ and $-10\%$ of the reference inlet value, for carbon dioxide and air plasmas respectively.

The results of this analysis are presented in Figs. 19(a) and 19(b), where are shown the heat ux maps corresponding to the conditions de ned in Ref. [58], for both air and carbon dioxide. The results show an important in uence on the stagnation point heat ux for carbon dioxide mixtures. The reason of these differences can be explained from the analysis of species concentration showed in Fig. 19(c) for a fully catalytic cold wall. Indeed, the increase of oxygen outer edge fraction reduces the amount of carbon available for $CO_2$ recombination at the

surface, this leading to a lower heat ux. This is more evident for high values of recombination probabilities, where almost the same effect on wall heat ux is observed in the whole temperature range considered. As the recombination probability is reduced the in uence of the outer edge elemental fraction decreases as well, and a higher in uence is observed for cold wall conditions, where recombination is enhanced by the bulk chemistry owing to the low temperature.
As far as air mixtures are concerned, the effects on wall heat ux are essentially negligible. Indeed the lines of Fig. 19(b) are superposed for all values of catalycity in the temperature range investigated. The quite low in u-ence on heat ux can be explained by the analysis of the species mass fraction pro les of Fig. 19(d). Indeed the perturbation of the elements fraction shifts slightly the concentration of $N_2$, N, and O at the outer edge without altering too much the stagnation line chemistry.
The analysis carried out in this section shows therefore that, especially for Mars entry applications, the outer edge elemental fractions play an important role in the determination of the heat ux map and therefore in the extrapolation of the TPS material catalycity.

# 6 Conclusions

In this section the main achievements of the present research are recalled following the structure of this manuscript with the aim to summarize the contributions brought to the modeling of high enthalpy gases in the framework of a macroscopic methodology used ti estimate the catalytic properties of thermal protection materials.

## 6.1 Theory of reacting mixtures under Local Thermodynamic Equilibrium

A series of new elemental transport coefficients have been presented for mixtures under thermochemical equilibrium conditions. They allow to reduce the equations of chemically reacting o ws in LTE to an elegant system consisting of the conventional Navier-Stokes equations (mass, momentum, energy) complemented by an advection-diffusion equation for the mass fraction of each chemical element in the mixture. The obtained formalism is in closed form in the sense that diffusive ux es are directly expressed in terms of gradients of the solution unknowns, unlike other formulations in which these ux es are obtained in an implicit manner, by solving the full system of Stefan-Maxwell equations. In the case of mixtures containing neutral components, assuming local neutrality and absence of current, we have introduced the following new transport properties : the elemental multicomponent ($D_{eq}$) and thermal demixing ($D_e^T$) diffusion coefficients, the thermal demixing conductivity ($\lambda_D$), the elemental heat transfer coefficients ($\lambda_{EL}^e$). We refer the interested reader to Ref. [57] for further details about the extension of this formalism composed of both neutral ad charged components.

## 6.2 Elemental diffusion along the stagnation line

To verify the importance of elemental diffusion phenomena and to assess the performances of the theory presented in Sec. 2, we focused on a 8-species $CO_2/N_2$ mixture containing three elements (C, N, O). This analysis was based on the use of the transport properties previously presented, which required the computation of nine elemental multicomponent and three thermal demixing coefficients, the demixing thermal conductivity and three elemental heat transfer coefficients, in addition to the 'standard' LTE transport properties.
The results of this study represent the rst attempt to compute thermal demixing and multicomponent diffusion coefficients as well as elemental heat transfer coefficients and thermal demixing conductivity for a mixture of heteronuclear components containing three elements. This proves the generality of the proposed formulation and clearly represents an improvement with respect to previous formulations available in the literature. In addition, the results obtained with the proposed closed form of the equations coincide with those obtained using an implicit formulation, indicating the correctness of the new formulation.
Finally, after a critical analysis of the results, we noticed how complex elemental concentration and heat ux patterns can be easily explained by examining graphs of LTE transport coefficients that arise from the new proposed LTE formulation.

## 6.3 Elemental diffusion in inductive coupled plasmas

In Sec. 4, we extended our analysis of elemental diffusion considering the investigation of air and carbon dioxide inductively coupled plasma o ws for application to Earth and Mars entry. To verify the validity of one of the major hypothesis of the IPM methodology, i.e. the existence of equilibrium conditions within ICP facilities, we considered both the equilibrium and the non equilibrium form of the governing equations. The numerical solution of these equations led to a detailed analysis of the o w behavior within the torch for air and $CO_2$ mixtures and then of the jet o wing into the test chamber for air mixtures.

Firstly, we presented original carbon dioxide plasma o w simulations under equilibrium considering both constant and variable elemental fraction conditions. A critical analysis of these results shows that for an inlet carbon volumetric fraction of ~ 33% :

- the solution, under chemical equilibrium, of an additional set of elemental continuity equations for oxygen and carbon shows the presence of important variations in the elemental composition.
- The amount of demixing observed for the operating conditions considered is characterized by a maximum increase to ~ 38% and a decrease to ~ 28% of the carbon elemental fraction.
- The effects of these variations in the elemental fraction on the species evolution is much higher than for air o ws. Indeed, at the outlet of the torch, important differences are observed between the species radial pro les obtained under equilibrium with constant and variable elemental fractions.
- The in uence of demixing on the temperature prediction is much higher for $CO_2$ o ws than for air. At the torch exit, neglecting elemental diffusion a maximum relative error of ~ 40% is observed for $r$ ~5.8 cm, while on the axis it decreases sharply to ~ 2%.

Secondly, we turned our attention to the analysis of air plasma flows both in the torch and in the chamber of the VKI-Plasmatron. Two operating pressures have been investigated corresponding to 5 kPa and 30 kPa. In addition, the three chemical regimes used to analyze air plasmas within the torch have been considered and for the description of chemical non equilibrium, two finite rate chemistry models have been selected as representative of Earth atmosphere chemistry.
The analysis of these results leads us to the following conclusions :

- for the low pressure case (5 kPa), we observe a certain influence of the finite rate chemistry model on the prediction of the flow behavior within the torch, while, as we move towards the test chamber, the flow predictions rapidly match leading to almost negligible discrepancies ~ 30 cm after the torch.
- Non equilibrium effects are observed within the torch for the 5 kPa operating pressure. In the jet, the non equilibrium results are rather close to the equilibrium ones, provided that elemental demixing is taken into account.
- The consequence of increasing the operating pressure is to sharply decrease the differences between the equilibrium and non equilibrium predictions. These differences are very small for the low pressure case (5 kPa) and they become negligible for the high pressure case (30 kPa), especially in the jet.

The major result of this analysis consists in the fact that, for the purpose of TPM testing, the costly simulation of chemical non equilibrium ICP flows, both in the torch and in the test chamber, can be avoided for sufficiently high pressures. Indeed the same accuracy can be reached relying on the numerical simulation of a more compact thermochemical equilibrium formalism based on the solution of an additional set of elemental advection diffusion equations, free of stiff source terms. In addition, because of the important elemental fraction variations observed as a result of both air and carbon dioxide plasma flow simulation, it appears desirable to add the elemental fractions at the stagnation line outer edge to the list of non dimensional parameters defined in the framework of the IPM methodology.

## 6.4 Practical application to TPM testing

Following the results obtained in the previous sections, we focused our interest on the analysis of stagnation line flows for application to TPS testing. To this end, both air and carbon dioxide mixtures have been analyzed considering only neutral components.

In our simulations, two models (Park [52] and McKenzie [44]) for the description of finite rate chemistry for a carbon dioxide mixtures of neutral species have been tested and important differences in the results have been observed. Then, our attention has been attracted by the heterogeneous recombination processes taking place on the surface of TPM samples. During our investigation, some unexpected flaws of the Scott [69] formulation have been discovered. To overcome them, an alternative model has been proposed and successfully tested.
The main outcome of the analysis of the results obtained with this new gas/surface interaction model reads as follows :

- a deeper description of the theoretical relation between a fully catalytic surface and the related equilibrium conditions is presented;
- we have shown that the constant elemental fraction assumption may contradict the hypothesis of equal effective recombination probability;
- we have shown that a non equilibrium model of a carbon dioxide stagnation line o w based on the constant elemental fraction assumption is in contrast with the equal recombination probability for CO and O involved in the formation of $CO_2$ and $O_2$ at the wall;
- we have shown that the equal recombination probability hypothesis may not be compatible with the local wall conditions;
- we have veri ed the in uence of the outer edge elemental fractions on the stagnation point heat ux. This in uence, rather important for carbon dioxide mixtures, con rms the necessity to add the them to the list of parameters of the methodology developed at the IPM suited for the estimation of catalytic properties of TPS materials, especially for Mars entry applications.

## References

[1] J. D. Anderson. *Hypersonic and high temperature gas dynamics.* McGraw-Hill, New York, 1989.

[2] C. O. Asma and O. Chazot. Trajectory simulation and catalycity determination for expert vehicle. In *Fifth European Symposium on Aerothermodynamics for Space Vehicles*, Cologne (Germany), 8-11 November 2004.

[3] P. Barbante, O. Chazot, and G. Degrez. Flight extrapolation of wind tunnel data for the determination of TPS materials catalycity. In *2nd International Symposium on Atmospheric Reentry Vehicles and Systems*, Arcachon, France, March 26-29 2001.

[4] P. F. Barbante. *Accurate and Efficient Modeling of High Temperature Nonequilibrium Air Flows.* PhD thesis, von Karman Institute, Rhode-Saint-Genèse, Belgium, 2001.

[5] B. Bottin, M. Carbonaro, O. Chazot, G. Degrez, D. Vanden Abeele, P. F. Barbante, S. Paris, V. Vanderhaegen, T. Magin, and M. Playez. The plasmatron and beyond: a decade of aerothermal plasma testing at the von karman institute. In *XXVI International Conference on Phenomena in Ionized Gases (ICPIG 2003)*, Greifswald, Germany, July 15- 20 2003.

[6] B. Bottin, O. Chazot, M. Carbonaro, V. Van der Haegen, and S. Paris. The VKI plasmatron characteristics and performance. In J. M. Charbonnier and G. S. R. Sarma, editors, *Measurement Techniques for High Temperature and Plasma Flows*, von Karman Institute for Fluid Dynamics, 1999. NATO-RTO-EN 8.

[7] R. S. Brokaw. Thermal conductivity of gas mixtures in chemical equilibrium. II. *Journal of Chemical Physics*, 32(4):1005, 1960.

[8] D. Bruno, M. Capitelli, E. Kustova, and E. Nagnibeda. Non-equilibrium vibrational distributions and transport coefficients of N2(v)-N mixtures. *Chemical Physics Letters*, 308(5-6):463–472, July 1999.

[9] J. N. Butler and R. S. Brokaw. Thermal conductivity of gas mixtures in chemical equilibrium. *Journal of Chemical Physics*, 26(6):1636, 1957.

[10] M. Capitelli, G. Colonna, D. Giordano, E. Kustova, E. Nagnibeda, M. Tuttafesta, and D. Bruno. *Mathematical Modelling*, 11(2):45, 1999.

[11] J. M. Charbonnier, J. Couzi, W. Dieudonne, and J. L. Verant. Workshop 2003 " radiation of high temperature gas", TC3 : De nition of an axially symmetric testcase for high temperature gas radiationprediction in Mars atmosphere entry. Technical report, CNES, Centre de Toulouse, Toulouse, France, May 2003. NG104-07-TF-001-CNES.

[12] O. Chazot, S. Paris, P. Collin, M. Bickel, and T. Ullman. TPS testing and catalycity determination in the VKI plasmatron facility. In *3rd International Symposium on Atmospheric Reentry Vehicles and Systems*, Arcachon, France, March 2003.

[13] O. Chazot, J. M. Pereira Gomes, and M. Carbonaro. Characterization of a 'mini-plasmatron' facility by pitot probe measurements. In *29th AIAA Plasmadynamics and Lasers Conference*, Albuquerque, NM, June, 15-18 1998. AIAA-1998-2478.

[14] G. Colonna, M. Tuttafesta, M. Capitelli, and D. Giordano. In uence of dissociation rates on the state-to-state vibrational kinetics in nozzle expansions. In CEPADUES, editor, *Rarefied Gas Dynamics 21*, volume 2, page 281, Toulouse, France, 1999.

[15] Marta de la Llave PLATA, O. Chazot, T. Magin, G. Degrez, and A. F. Kolesnikov. Application and analysis of a methodology for the determination of TPS catalytic properties. In *2nd International Symposium on Atmospheric Reentry Vehicles and Systems*, Arcachon, France, March 26-29 2001.

[16] G. Degrez, P. Barbante, M. de la Llave, T. Magin, and O. Chazot. Determination of the catalytic properties of TPS materials in the VKI ICP facilities. In *ECCOMAS Computational Fluid Dynamics Conference 2001*, pages 162–167, Swansea, Wales, UK, 4-7 September 2001.

[17] G. Degrez, D. Vanden Abeele, P. Barbante, and B. Bottin. Numerical simulation of inductively coupled plasma o ws under chemical non equilibrium. *International Journal of Numerical Methods in Heat and Fluid Flow*, 14(4):538–558, 2004.

[18] A. Ern and V. Giovangigli. The kinetic chemical equlibrium regime. *Physica A*, 260:49–72, 1998.

[19] P. Rini et al. Assessment of thermodynamics, transport, and chemical properties for $CO_2$ o ws. Contract report, von Karman Institute for Fluid Dynamics, Rhode-Saint-Genèse, Belgium, August 2002. MSR02-TNP4.1-VKI.

[20] P. Rini et al. Evaluation of numerical codes for high enthalpy $CO_2$ o ws. Technical report, von Karman Institute for Fluid Dynamics, Rhode-Saint-Genèse, Belgium, August 2002. MSR02-TNP6.1-VKI.

[21] J. A. Fay and F. R. Riddell. Theory of stagnation point heat transfer in dissociated air. *Journal of the Aeronautical Science*, 1958.

[22] J. H. Ferziger and H. G. Kaper. *Mathematical Theory of Transport Processes in Gases*. North-Holland, Amsterdam, 1972.

[23] W. Frie. Thermodynamics of irreversible processes and the force equations of schluter. *Zeitschrift für Physik*, 162:61–68, 1961.

[24] W. Frie and H. Maecker. Mass separation by diffusion of reacting gases. *Zeitschrift für Physik*, 162:69–83, 1961.

[25] W. Frie and H. Maecker. Dynamics of reacting gases. *Zeitschrift für Physik*, 168:206–232, 1962.

[26] W. Frie and H. Maecker. Demixing effects in mixtures of ionizing atomic gases. *Zeitschrift für Physik*, 172:99–117, 1963.

[27] A. Garcia, O. Chazot, and D. Fletcher. Investigation in plasmatron facilities on catalycity determination. In *4th European symposium for space vehicles*, Capua, Italy, October 16-18 2001.

[28] A. M. Garcia. Catalycity effects in plasmatron tests. Technical report, von Karman Institute for Fluid Dynamics, Rhode-Saint-Genèse, Belgium, June 2001. VKI PR 2001-12.

[29] P. A. Gnoffo, R. N. Gupta, and J. L. Shinn. Conservation equations and physical models for hypersonic air o ws in thermal and chemical nonequilibrium. Technical Paper 2867, NASA (Langley), Virginia, 1989.

[30] A. Groß. *Theoretical Surface Science - A microscopic perspective*. Springer Verlag, 2002.

[31] A. Groß. Introduction to theoretical surface science. In *Experiment, Modelings and Simulation of gas-surface interactions for reactive flows in hypersonic flights*, Rhode Saint Genèse, February 2006. von Karman Institute for Fluid Dynamics. VKI-LS.

[32] J. O. Hirschfelder, C. F. Curtiss, and R. B. Bird. *Molecular Theory of Gases and Liquids*. Wiley, New York, 1964.

[33] IPM. Surface catalysis determination for earth and mars atmospheres re-entry vehicles: Microscopic vs macroscopic methods. Technical report, INTAS/CNES, 2005. Project 03-53-5117.

[34] A. F. Kolesnikov. Combined measurements and computations of high enthalpy and plasma o ws for determination TPM surface catalycity. In J. M. Charbonnier and G. S. R. Sarma, editors, *Measurements Techniques for High Enthalpy and Plasma Flows*, pages 8A 1–16, Rhode-St-Genèse Belgium, Oct. 1999. NATO-RTO-EN.

[35] A. F. Kolesnikov. Extrapolation from high enthalpy tests to ight based on the concept of local heat transfer simulation. In J. M. Charbonnier and G. S. R. Sarma, editors, *Measurements Techniques for High Enthalpy and Plasma Flows*, pages 8A 1–14, Rhode-St-Genèse Belgium, Oct. 1999. NATO-RTO-EN.

[36] A. F. Kolesnikov. Calculation of heat transfer and effective atoms recombination probability $\gamma_w$ in dissociated air jet of the induction plasmatron.(user manual). Technical report, Research Institute of Mechanics at Moscow State University, Moscow, March 2000.

[37] A. F. Kolesnikov. An efficient modeling stagnation point heat transfer for subsonic aerothermal test conditions. In *Technical note 200*, Rhode-St-Genèse Belgium, January 2001. VKI-TN-200.

[38] A. F. Kolesnikov and L. Marraffa. An analysis of stagnation point thermochemical simulation by plasmatron for Mars probe. In *33rd Thermophysics Conference*, Norfolk, VA, June-July 1999. AIAA Paper 99-3564.

[39] A. F. Kolesnikov, I. S. Pershin, S. A. Vasil'evskii, and M. I. Yakushin. Study of quartz surface catalycity in dissociated carbon dioxide subsonic o ws. *Journal of Spacecraft and Rockets*, 37:573–579, September-October 2000.

[40] A. F. Kolesnikov, M. I. Yakushin, I. S. Pershin, S. A. Vasil'evskii, O. Chazot, B. Vancrayenest, and J. Muylaert. Comparative study of surface catalycity under subsonic air test conditions. In *4th European symposium for space vehicles*, Capua, Italy, October 16-18 2001.

[41] V. L. Kovalev and O. N. Suslov. Diffusion separation of chemical elements on a catalytic surface. *Fluid Dynamics*, 23(4):579–585, 1988.

[42] E. Kustova and E. Nagnibeda. State-to-state approach in the transport kinetic theory. In CEPADUES, editor, *Rarefied Gas Dynamics 21*, volume 1, page 231, Toulouse, France, 1999.

[43] T. Magin. *A model for Inductive Plasma Wind Tunnels*. PhD thesis, von Karman Institute for Fluid Dynamics, St.-Genesius-Rode, Belgium, 2004.

[44] R. L. McKenzie. An estimate of the chemical kinetics behind normal shock waves in mixtures of carbon dioxide. NASA TN D-3287, Ames Research Center, Moffett Field, CA, 1966.

[45] A. B. Murphy. Combined diffusion coefficients in equilibrium mixtures of dissociating gases. *Journal of Chemical Physics*, 99(2):1340, 1993.

[46] A. B. Murphy. Diffusion in equilibrium mixtures of ionized gases. *Physical Review E (Statistical, Nonlinear, and Soft Matter Physics)*, 48(5):3594, 1993.

[47] A. B. Murphy. Demixing due to frictional forces in an electric arc. *Physical Review Letters*, 73(13):1797, 1994.

[48] A. B. Murphy. Demixing in free-burning arcs. *Physical Review E (Statistical, Nonlinear, and Soft Matter Physics)*, 55:7473, 1997.

[49] E. Nagnibeda. The structure of the relaxation zone behind shock waves in the reacting gas o ws. In J. Hunt, editor, *Aerothermodynamics for Space Vehicles*, Noordwijk, The Netherlands, 1995. ESTEC, ESA Publication Division.

[50] E. Nagnibeda. Kinetic theory of transport processes and thermodynamics, polyatomic molecules. In Fletcher *et al.*, editor, *Physico-chemical models for high enthalpy and plasma flows*, Rhode-Saint-Genése, Belgium, 2002. von Karman Institute for Fluid Dynamics. VKI LS 2002-07.

[51] M. Panesi. Numerical simulation of non equilibrium plasma o ws. Technical report, von Karman Institute for Fluid Dynamics, Rhode-Saint-Genèse, Belgium, June 2005. VKI PR 2005-23.

[52] C. Park, J. T. Howe, and R. L. Jaffe. Review of chemical-kinetic problems of future nasa mission, II: Mars entries. *Journal of Thermophysics and Heat Transfer*, 8(1):9–23, 1994.

[53] C. Park, R. L. Jaffe, and H. Partridge. Chemical-kinetic parameters of hyperbolic earth entry. *Journal of Thermophysics and Heat Transfer*, 15(1):76–90, 2001.

[54] M. Balat Pichelin et al. Molecular dynamic simulation and experimental determination of the recombination of atomic oxygen on silica polymorphs at 1000 K. In *4th International Symposium Atmospheric Reentry Vehicles and Systems*, Arcachon (France), 21-23 March 2005.

[55] J. Richter. Über diffusionsvorgaenge in lichtboegen. *Zeitschrift für Astrophysik*, 53:262–272, 1961.

[56] P. Rini. Numerical simulation of equilibrium and non equilibrium $CO_2$ plasma o ws. Technical report, von Karman Institute for Fluid Dynamics, Rhode-Saint-Genèse, Belgium, June 2002. VKI PR 2002-22.

[57] P. Rini. *Analysis of differential diffusion phenomena in high enthalpy flows, with application to thermal protection material testing in ICP facilities*. PhD thesis, von Karman Institute for Fluid Dynamics, St.-Genesius-Rode, Belgium, 2006.

[58] P. Rini and G. Degrez. Elemental demixing along both air and carbon dioxide stagnation line o ws. *Journal of Thermophysics and Heat Transfer*, 18(4):511–518, 2004.

[59] P. Rini, A. Garcia, T. Magin, and G. Degrez. Numerical simulation of $CO_2$ stagnation line o ws with catalyzed surface reactions. *Journal Thermophysics and Heat Transfer*, 18(1):114–121, 2004.

[60] P. Rini, T. Magin, G. Degrez, and D. Fletcher. Numerical Simulation of Non Equilibrium Hypersonic $CO_2$ o ws for mars entry application. In $3^{rd}$ *International Symposium Atmospheric Reentry Vehicles and Systems*, Arcachon, France, March 2003.

[61] P. Rini, N. Nannipieri, O. Chazot, and G. Degrez. Numerical simulation of thermochemical equilibrium boundary layers. In *6th National Congress on Theoretical and Applied Mechanics*, Gent, Belgium, 26-27 May 2003.

[62] P. Rini, D. Vanden Abeele, and G. Degrez. Closed form for the equations of chemically reacting o ws under local thermodynamic equilibrium. *Physical Review E (Statistical, Nonlinear, and Soft Matter Physics)*, 72(1):011204, 2005.

[63] P. Rini, D. Vanden Abeele, and G. Degrez. Analysis of diffusion phenomena in lte mixtures with applications to $CO_2/N_2$mixtures. *to be submitted to the Journal of Thermophysics and Heat Transfer*, 2006.

[64] P. Rini, D. Vanden Abeele, and G. Degrez. Elemental demixing in inductively coupled air plasmas torches at high pressures. *Journal of Thermophysics and Heat Transfer*, 20(1):31–40, 2006.

[65] P. Rini, S. A . Vasil'evskii, A. F. Kolesnikov, O. Chazot, and G. Degrez. Inductively coupled $co_2$ plasma o ws: a code-to-code comparison. In *4th International Symposium Atmospheric Reentry Vehicles and Systems*, Arcachon (France), 21-23 March 2005.

[66] P. Rini, S. A. Vasil'evskii, A. F. Kolesnikov, O. Chazot, and G. Degrez. $CO_2$ stagnation line o w simulation for mars entry applications. In *38th AIAA Thermophysics Conference*, Toronto (CA), 6-8 Jun 2005.

[67] G. S. R. Sarma. Physico-chemical modeling in hypersonic o w simulation. *Progress in Aerospace Sciences*, 36(3-4):281–349, 2000.

[68] S.A.Vasil'evskii. Calculation of flow and heat transfer at blunt body stagnation line with account for the diffusion of elements and higher approximations for transport coefficients. In *Investigations of hypersonic aerodynamics and heat transfer with account for non equilibrium chemical reactions*, pages 30–45, Moscow, 1987. Moscow State University publishing.

[69] D. C. Scott. Catalytic boundary conditions in nonequilibrium flow. *Proceeding of the IUTAM Symposium Marseille*, pages 298–305, 1992.

[70] O. N. Suslov, G. A. Tirsky, and V. V. Shchennikov. Flows of Multicomponent Ionized Mixtures in Chemical Equilibrium. Description within the Framework of the Navier-Stokes and Prandtl Equations. In *Prikl. Mekh. and Tekhn. Fiz.*, 1971.

[71] J. Thömel. Local heat transfer simulation of air and $CO_2$. Technical report, von Karman Institute for Fluid Dynamics, Rhode-Saint-Genèse, Belgium, June 2005. VKI PR 2005-01.

[72] G. A. Tirsky. Up-to-date gasdynamic models of hypersonic aerodynamics and heat transfer with real gas properties. *Annual Review of Fluid Mechanics*, 25:151–181, 1993.

[73] G. A. Tirsky. The hydrodynamic equations for chemically equilibrium flows of a multielement plasma with exact transport coefficients. *Journal of Applied Mathematics and Mechanics*, 63(6):841–861, 1999.

[74] H. W. P. van der Heijden. *Modeling of radiative transfer in light sources*. PhD thesis, Technische Universiteit Eindhoven, Eindhoven, the Netherlands, January 2003.

[75] D. Vanden Abeele. *An Efficient Computational Model for Inductively Coupled Air Plasma Flows under Thermal and Chemical Non-Equilibrium*. PhD thesis, von Karman Institute, Rhode-Saint-Genèse, Belgium, 2000.

[76] D. Vanden Abeele and G. Degrez. Efficient computational model for inductive plasma flows. *AIAA Journal*, 38(2):234–242, 2000.

[77] S. A. Vasil'evskii, A. F. Kolesnikov, and M. I. Yakushin. Mathematical models for plasma and gas flows in induction plasmatrons. In *Molecular Physics and Hypersonic Flows (Ed. M. Capitelli)*, pages 495–504, Kluwer, Dordrecht, the Netherlands, 1996.

[78] S.A. Vasil'evskii and G.A. Tirsky. Influence of multicomponent diffusion and higher approximations for the transport coefficients on the heat flux to blunt body at hypersonic flight. In *Applied aerodynamics of vehicles*, pages 100–103, Kiev, 1984. Naukova dumka publishing.

[79] W. G. Vincenti and C. H. Kruger. *Introduction to Physical Gas Dynamics*. John Wiley and Sons, New York, 1965.